An assembly model for the autophagy initiation complex

by

Daniel Fernando Ramirez Montero

Sc.B. Biochemistry and Molecular Biology
Brown University, 2016

SUBMITTED TO THE DEPARTMENT OF BIOLOGY IN PARTIAL FULLFILLMENT OF THE REQUIREMENTS FOR THE DEGREE OF

MASTER OF SCIENCE IN BIOLOGY
AT THE
MASSACHUSETTS INSTITUTE OF TECHNOLOGY

SEPTEMBER 2019

Signature of Author: _____
Daniel Fernando Ramirez Montero
Department of Biology
August 8, 2019

Certified by: _____
Joseph H. Davis
Assistant Professor

Accepted by: _____
Stephen P. Bell
Uncas and Helen Whitaker Professor of Biology
Investigator, Howard Hughes Medical Institute
Co-Director, Biology Graduate Committee

An assembly model for the autophagy initiation complex

by

Daniel Fernando Ramirez Montero

Submitted to the Department of Biology on August 8, 2019 in partial fulfillment
of the requirements for the degree of Master of Science in Biology at the
Massachusetts Institute of Technology

Abstract

Autophagy is a highly conserved eukaryotic homeostasis process that facilitates degradation of intracellular components. During times of starvation, autophagy is vital in replenishing pools of biosynthetic precursors through degradation of these cytosolic components, and it also plays key roles in responding to cytotoxic stress as it acts to specifically degrade damaged organelles, aggregated proteins, and pathogens. This is achieved by the formation of an autophagosome, a double membrane organelle that engulfs cytoplasmic components and then fuses with the vacuole or the lysosome leading to degradation of the engulfed components. Of note, defects in autophagy have been genetically linked with cancer, neurodegeneration, inflammation and aging, highlighting the importance of deeply understanding this process.

Although several genetic screens have enumerated the proteins required for autophagy, our mechanistic understanding of how these proteins interact and function in autophagy is very limited. In this work, I focus on the most upstream autophagy protein complex, called the Atg1 complex or autophagy initiation complex (AIC), which binds high curvature lipid vesicles and is thought to catalyze their fusion to initiate autophagosome biogenesis. In chapters 1-4 of this work, I review what is currently known about different steps of the mechanism of AIC formation, its interactions with lipid vesicles and its putative functional role in initiating autophagosome formation, highlighting outstanding questions throughout. Finally, in Chapter 5, I describe my efforts to develop a new single-molecule approach to study the mechanism of AIC assembly, and discuss the important unanswered questions that this new approach may allow us to address.

Thesis Supervisor: Joseph H. Davis

Title: Assistant Professor of Biology

Acknowledgements

First of all, I would like to thank my advisor, Joey Davis, for his support and mentoring during my time in his group, for always gently pushing me to become a better scientist and for believing in me from the beginning. Most importantly, I want to thank Joey for his friendship, which I will always cherish.

I would also like to thank everyone in the Davis Laboratory for always brightening up my day with a joke, a smile or a friendly bark, and for having made me feel welcomed and cared for from the very first day. In particular, I would like to thank Andrew Grassetti for his friendship and for teaching me by example that kindness is the best quality a scientist can have, Sam Webster for constantly brightening up my day with her fun facts and jokes, and Bertina Telusma for the impromptu salsa lessons. I will miss you guys dearly.

I also want to sincerely thank professors Steve Bell and Amy Keating for their support during this time, for constantly reminding me that I was not alone, and for helping me discover my love for biophysics.

I also thank my parents and siblings for their love and support during this time and for teaching me that no ocean or border can separate us. Your constant text messages and phone calls helped me keep going when I did not think that I could.

Finally, I want to thank my partner and best friend, Diego López Barreiro, for all his love and support during this time, without which I could not have reached this point. Thank you for constantly inspiring me to become a better scientist and person, and for always bringing happiness to my life, Dieguín.

Table of contents

Table of figures

Preface

Autophagy is a highly conserved (Mizushima, 2010; Mizushima et al., 2011; Nakatogawa et al., 2009) homeostasis process whereby cells degrade intracellular proteins, organelles, or pathogens. During times of starvation, autophagy is vital in replenishing pools of biosynthetic precursors through degradation of these cytosolic components; it also plays key roles in responding to cytotoxic stress as it acts to specifically degrade damaged organelles, aggregated proteins, and pathogens (Morishita and Mizushima, 2019). Highlighting the importance of this process, defects in autophagy have been linked to neurodegeneration, cancer, infection and aging (Galluzzi et al., 2015; Gomes and Dikic, 2014; Menzies et al., 2015; Mizushima and Komatsu, 2011). Much of our molecular understanding of autophagy comes from seminal genetic screens carried out in the budding yeast *Saccharomyces cerevisiae* in the 1990s, which lead to a nearly complete inventory of 42 autophagy-related (Atg) proteins (Kabeya et al., 2007; Kawamata et al., 2005; Klionsky et al., 2003; Mizushima et al., 2011; Morishita and Mizushima, 2019; Tsukada and Ohsumi, 1993). In contrast, the human autophagy protein inventory is incomplete with new components constantly being uncovered. Because our understanding of human autophagy is more limited (Bento et al., 2016), I will focus on yeast autophagy in this work.

Autophagy can be triggered by multiple cellular stresses (Hurley and Young, 2017; Klionsky, 2007; Mizushima et al., 2011) including starvation-induced autophagy, which is the best characterized (Fujioka et al., 2014; Kabeya et al., 2009; Kamada et al., 2000; Nakatogawa et al., 2009) and the focus of this work. In yeast, nutrient starvation induces the formation of a protein complex known as the Atg1 complex or autophagy initiation complex (AIC) which assembles in a punctate structure at a perivacuolar location known as the phagophore assembly site (PAS) (Kawamata et al., 2008; Noda and Inagaki, 2015; Suzuki et al., 2001, 2007). There, the AIC recruits small membrane vesicles (Rao et al., 2016; Reggiori et al., 2005; Sekito et al., 2009; Suzuki et al., 2007, 2015) and is thought to catalyze their fusion (Rao et al., 2016; Yamamoto et al., 2012), which leads to formation of a cup-shaped membrane structure known as the phagophore. The growing phagophore then engulfs cytoplasmic cargo, forming a double-membrane vesicle known as the autophagosome (Hurley and Young, 2017). Next, the autophagosomal outer membrane fuses with the vacuole exposing the inner membrane and the engulfed cargo to the degradative capacity

of vacuolar hydrolases, which degrade these components to their biosynthetic precursors (*e.g.* amino acids, nucleotides, lipids). Release of these biosynthetic precursors replenishes their cytosolic pools and acts to repress autophagy through a negative feedback loop (Kaur and Debnath, 2015; Morishita and Mizushima, 2019; Onodera and Ohsumi, 2005). Given the efficacy of the lysosomal system in degrading autophagic cargo, the pathway is highly regulated (He, 2010) and many factors are dedicated to substrate selection (Morishita and Mizushima, 2019).

Starvation-induced autophagic substrate selection can be divided into three categories: non-selective, in which autophagosomes engulf cargos irrespectively of their identity; exclusive, in which an autophagosome specifically and exclusively engulfs a single cargo using adaptor proteins (Lynch-Day and Klionsky, 2010; Morishita and Mizushima, 2019); and selectively, in which a single autophagosomes contains both non-selective cargoes as well as specific targets that have been selected using dedicated adaptors proteins (Lynch-Day and Klionsky, 2010). These subdivisions of starvation-induced autophagy, however, have not been thoroughly studied in the existing starvation-induced autophagy literature and, for this reason, I will not differentiate between them here. Importantly, though I aim to detail common features of these three types of substrate selection in starvation-induced autophagy, further experimental work is required to confirm that the observations that I highlight here are in fact shared by the three categories of substrate selection.

Of the 42 known autophagy-related proteins, 18 are involved in autophagosome formation and they have been classified into six functional groups (Noda and Inagaki, 2015) that are thought to arrive at the PAS in a specific order (Suzuki et al., 2007). These groups include: the AIC; the transmembrane protein Atg9; the autophagy-specific phosphatidylinositol 3-kinase (PI3K) complex; the Atg2-Atg18 complex; and the Atg8 and Atg12 conjugation systems. In this work, I will specifically focus on the AIC and on our current mechanistic understanding of its assembly and function.

The AIC is made up of 5 proteins: Atg1, Atg13, Atg17, Atg29 and Atg31 (Köfinger et al., 2015). While few mechanistic biochemical studies have been performed, the AIC is generally thought to assemble from two pre-assembled subcomplexes, Atg1/Atg13 and Atg17/Atg29/Atg31 (Stjepanovic et al., 2014). The structure of this work is based on this model: in Chapter 1 and

Chapter 2, I focus on interactions within the Atg1/Atg13 and the Atg17/Atg29/Atg31 subcomplexes, respectively. In Chapter 3, I describe the interactions between these two subcomplexes that give rise to the active pentameric AIC. In Chapter 4, I discuss the recruitment of lipid vesicles and their potential fusion by the AIC. Finally, in Chapter 5, I describe the experimental progress that I have made towards developing a new single-molecule approach to study the AIC and discuss the important questions that this new approach may answer.

Chapter 1: Interactions between Atg1 and Atg13

The Atg1 complex, also known as the autophagy initiation complex (AIC), is the first autophagy-related protein complex that assembles upon starvation and it is composed of five proteins: Atg1, Atg13, Atg17, Atg29 and Atg31 (Chew LH et al., 2015; Fujioka et al., 2014; Köfinger et al., 2015; Rao et al., 2016; Stjepanovic et al., 2014). In yeast, the AIC assembles at a perivacuolar punctate structure known as the phagophore assembly site (PAS) (Kawamata et al., 2008; Noda and Inagaki, 2015; Suzuki et al., 2001, 2007) (Figure 1a). Once assembled, the pentameric AIC recruits high-curvature membrane vesicles containing the only essential transmembrane autophagy protein, Atg9 (Noda et al., 2000; Rao et al., 2016; Reggiori et al., 2005; Sekito et al., 2009; Suzuki et al., 2007, 2015) (Figure 1b). The observation that these Atg9-loaded vesicles fuse at the PAS has led to the suggestion that the AIC catalyzes the fusion of Atg9-loaded vesicles and thereby initiates the formation of a cup-shaped membrane structure known as the phagophore (Rao et al., 2016; Yamamoto et al., 2012) (Figure 1c). The growing phagophore then engulfs cytoplasmic cargo, forming a double-membrane structure known as the autophagosome (Hurley and Young, 2017) (Figure 1d). Next, the autophagosomal outer membrane fuses with the vacuole (Figure 1e) exposing the inner membrane and the engulfed cargo to the degradative capacity of vacuolar hydrolases, which degrade these components to biosynthetic precursors such as amino acids, nucleotides, or lipids (Figure 1f). Release of these biosynthetic precursors

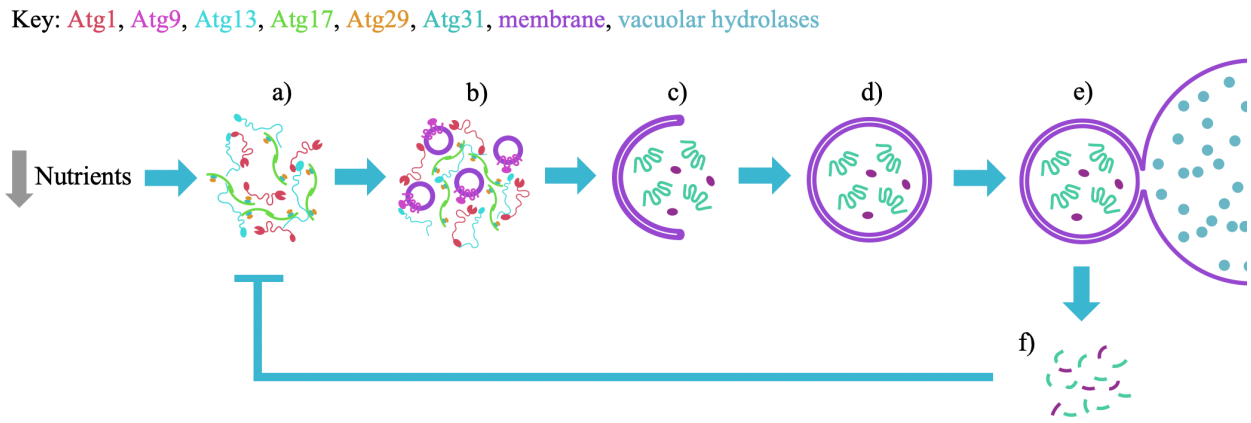

Figure 1: Overview of starvation-induced autophagy. Diagram shows key steps in starvation-induced autophagy. Starvation induces AIC assembly **(a)**. Upon assembly, the AIC recruits Atg9-loaded vesicles **(b)** and is thought to catalyze their fusion to start to form a phagophore, which elongates and engulfs a cytoplasmic cargo **(c)**. The phagophore eventually closes and forms an autophagosome **(d)**. Once the autophagosome is formed, its outer membrane fuses with the vacuole **(e)** and the vacuolar hydrolases degrade the autophagosome's cargo and inner membrane, releasing important biosynthetic precursors **(f)** that negatively feedback on the entire process.

replenishes their cytosolic pools and acts to repress autophagy through a negative feedback loop (Kaur and Debnath, 2015; Morishita and Mizushima, 2019; Onodera and Ohsumi, 2005). Given the efficacy of the lysosomal system in degrading autophagic cargo, this pathway is highly regulated (He, 2010) and many factors are dedicated to substrate selection (Morishita and Mizushima, 2019). Notably, whether the pentameric AIC is sufficient to mediate Atg9-loaded vesicle fusion remains an open question of debate. Irrespectively, proper AIC assembly at the PAS plays a vital role in initiating autophagy, which highlights the importance of understanding how the AIC assembles and how this assembly is regulated.

While few mechanistic studies have been performed, the AIC is thought to be assembled from two pre-assembled subcomplexes, Atg1/Atg13 and Atg17/Atg29/Atg31 (Stjepanovic et al., 2014). In this chapter, I will discuss the known interactions between Atg1 and its regulator, Atg13, and how these interactions give rise to the Atg1/Atg13 subcomplex. Finally, at the end of the chapter, I will briefly discuss Atg17, another regulator of Atg1 that cooperates with Atg13 in the activation of Atg1 (Yeh et al., 2010, 2011).

Atg1: A conserved kinase and scaffolding protein.

The Atg1 kinase is essential in autophagy and the only component of the AIC with known catalytic activity in addition to scaffolding functions (Chang and Neufeld, 2009; Cheong et al., 2008; Rao et al., 2016; Reggiori et al., 2004a). This dual catalytic/scaffolding role is of interest as the kinase domain could serve as a prime target for the development of broadly acting autophagy modulators with potential therapeutic benefit. This kinase domain resides at Atg1's N-terminus and is connected through a putative intrinsically disordered region (IDR) to an early autophagy targeting/tethering (EAT) motif (Ragusa et al., 2012) made up of two tandem microtubule-interacting and transport domains (tMIT) named

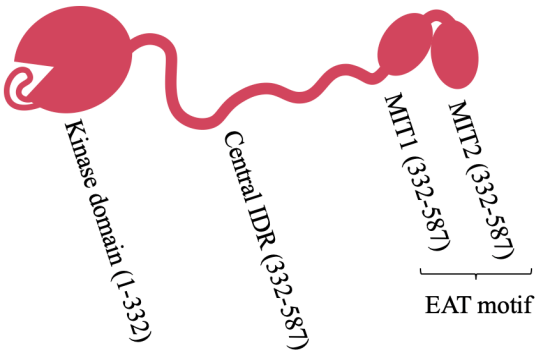

Figure 2: Architecture of Saccharomyces cerevisiae Atg1. Atg1 consists of an N-terminal kinase domain (including auto-inhibitory loop), followed by a central putatively disordered region and a C-terminal early autophagy targeting/tethering (EAT) motif, made up of two tandem microtubule-interacting and transport motifs (MIT1 and MIT2). Ovals represent structured regions and squiggles represent putatively disordered regions.

MIT1 and MIT2 (Fujioka et al., 2014) (Figure 2). The scaffolding and kinase functions of Atg1 are thought to be involved at distinct stages of autophagy (Cheong et al., 2008; Sekito et al., 2009). Indeed, the *scaffolding functions* of Atg1 are required for the recruitment of other AIC components to the PAS whereas the kinase domain is dispensable for PAS formation (Cheong et al., 2008; Kawamata et al., 2008). Instead, *kinase activity* is required for the recycling of other early autophagy components from the PAS, as evidenced by the fact that Atg9, Atg17 and Atg29 aberrantly accumulate at the PAS in the presence of Atg1 variants bearing catalytically inactive kinase domains (Cheong et al., 2008; Kawamata et al., 2008; Sekito et al., 2009; Shintani and Klionsky, 2004). Additionally, Atg1 kinase activity is essential for autophagy progression (Kamada et al., 2000) and it has been suggested to be responsible for the dissociation of the AIC into subcomplexes by phosphorylating other AIC components (Rao et al., 2016), suggesting an important role of Atg1 in auto-regulation of AIC formation. Thus, understanding Atg1 kinase activation might prove critical in understanding how several diseases and aging cause defects in autophagy (Galluzzi et al., 2015; Gomes and Dikic, 2014; Menzies et al., 2015; Mizushima and Komatsu, 2011). The activation of the Atg1 kinase activity requires other Atg proteins (Kabeya et al., 2005) that I will discuss in the following sections.

Atg13: A highly flexible scaffolding protein.

Atg13 consists of a Hop/Rev7/Mad2 (HORMA) domain at the N-terminus (Jao et al., 2013) and a putative C-terminal IDR (Figure 3). Atg13 is a conserved regulator of Atg1 kinase activity, is essential for autophagy, and is the only AIC component reported to directly bind Atg1 (Chew LH et al., 2015; Stephan et al., 2009). Although Atg13's HORMA domain is thought to be more structured than its IDR, the HORMA domain can readily undergo order-disordered transitions in physiological conditions (Yamamoto et al., 2016), suggesting that it may need a binding partner to stabilize the fold. Of note, HORMA domains in other proteins bind other HORMA domains (Qi et al., 2015), but the binding partner for *S. cerevisiae* Atg13 is not known. Finding this partner might be crucial in understanding how the HORMA domain is stabilized, which, as I will soon discuss, could play a role in recruiting Atg9-loaded vesicle to the PAS (Suzuki et al., 2015).

Vital autophagy initiation functions have been mapped throughout the Atg13 sequence. First, the N-terminal HORMA domain is thought to directly interact with Atg9 and to be primarily responsible for Atg9 recruitment to the PAS (Suzuki et al., 2015) (discussed in Chapter 4). Second, short sequences within the C-terminal IDR bind to conserved sites on the Atg17 scaffold protein (Chew LH et al., 2015; Fujioka et al., 2014; Yamamoto et al., 2016). Finally, additional contacts in the C-terminal IDR bind to Atg1 (Fujioka et al., 2014; Stjepanovic et al., 2014). Taken together, these Atg13 binding sites effectively link the Atg17/Atg29/Atg31 subcomplex to Atg9-loaded vesicles and to the Atg1 kinase (Stjepanovic et al., 2014). Moreover, Atg13 is thought to mediate crosslinking of multiple pentameric AICs (Yamamoto et al., 2016). As I will discuss in Chapter 3, this Atg13-mediated crosslinking increases the local concentrations of all the components of the AIC, which likely facilitates AIC assembly and Atg9-loaded vesicle fusion to start phagophore formation (further discussed in Chapter 4). In this chapter, however, I focus on the Atg1/Atg13 interactions, leaving the interactions between Atg13 and other AIC components for subsequent chapters.

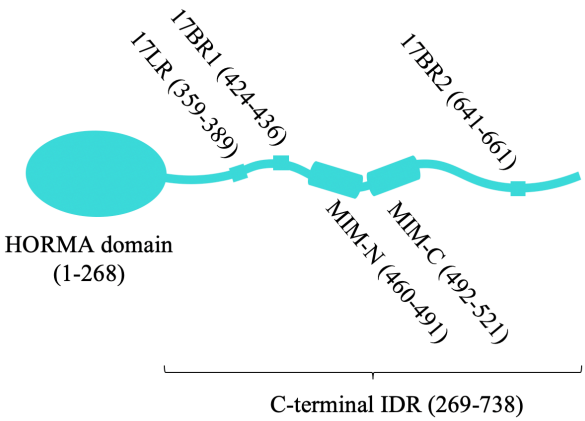

Figure 3: Architecture of Saccharomyces cerevisiae Atg13. HORMA domain contains Atg9 binding site; 17BR1, 17BR2 and 17LR are Atg17 binding motifs; MIM-N and MIM-C are binding Atg1 binding sites. 17BR1, 17BR2, 17LR, MIM-N and MIM-C contain serines thought to be phosphorylated by Tor.

Starvation-induced assembly of the Atg1/Atg13 sub-complex.

The formation of the AIC is a highly regulated step in autophagy (Chang and Neufeld, 2009; Kamada et al., 2000; Stephan et al., 2009), suggesting that it is an important decision point in the cell. Therefore, I predict that understanding which interactions within the AIC are regulated will provide us with important insights toward the development of therapeutic agents to modulate autophagy. Within Atg13's C-terminal IDR are two tandem MIT-interacting motifs (tMIM) named MIM-N and MIM-C, that interact with the tMIT motifs of Atg1 (Fujioka et al., 2014; Stjepanovic et al., 2014). The Atg1/Atg13 interaction is essential for autophagy (Kawamata et al., 2008) and it is mediated by binding of these motifs in an anti-parallel fashion: MIM-N (Atg13) binds MIT2 (Atg1) and MIM-C (Atg13) binds MIT1 (Atg1) (Fujioka et al., 2014). Of note, *in vitro* hydrogen-

deuterium exchange (HDX) experiments showed that Atg1's tMIT motif is highly dynamic in isolation but becomes more rigid upon binding to the Atg13's tMIMs (Stjepanovic et al., 2014), suggesting a potential role of this binding event in the stabilization of the Atg1^{tMIT} motif. This putative stabilization of Atg1^{tMIT} motif would be important because, as I will further discuss in Chapter 4, the Atg1^{tMIT} motif has been suggested to play a role in the selective recruitment of high curvature Atg9-loaded vesicles to the PAS (Ragusa et al., 2012; Rao et al., 2016). Additionally, having linked binding of two tandem motifs allows for tighter overall affinity through avidity effects and through the effects of tethering on the effective concentration of the individual motifs, while potentially allowing for more facile regulation, as both motifs could exchange and expose themselves to regulatory elements, such as the kinases and phosphatases that I will discuss in the following sections. Concordantly, isothermal titration calorimetry (ITC) experiments showed that, when compared in isolation, Atg13^{MIM-N} is a stronger binding site for Atg1^{tMIT} than Atg13^{MIM-C}; however, adding Atg13^{MIM-C} to Atg13^{MIM-N} greatly enhances the overall binding for Atg1^{tMIT} (Fujioka et al., 2014).

Both Atg1 and Atg13 are phosphoproteins whose phosphorylation states depend on the nutritional state of the cell, suggesting that they may be primary starvation sensors (Budovskaya et al., 2005; Stephan et al., 2009) (Figure 4). Under fed conditions, residues within Atg1's central IDR are phosphorylated by the (cyclic AMP)-dependent protein kinase (PKA) (Budovskaya et al., 2005). Upon carbon starvation, PKA is inactivated (Thevelein et al., 2000) and Atg1 is readily dephosphorylated by cellular phosphatases, which, through an unknown mechanism, results in recruitment of Atg1 to the PAS (Budovskaya et al., 2005). Similarly, Atg13 is phosphorylated by nutrient-dependent kinases PKA and Tor (target of rapamycin) under fed conditions and becomes

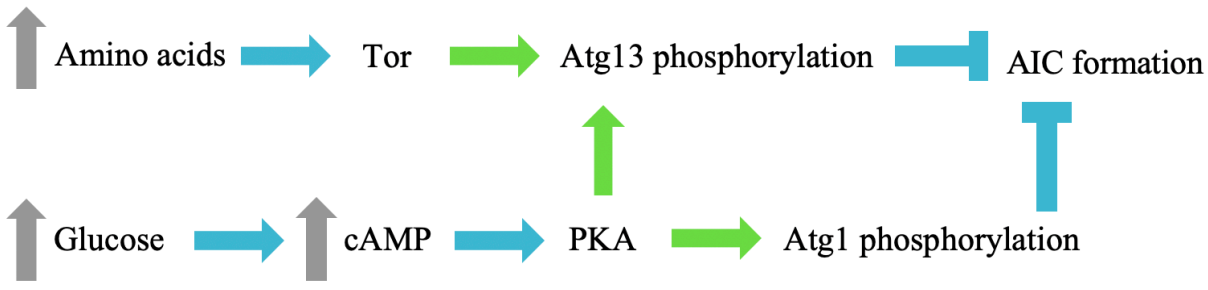

Figure 4: Carbon and nitrogen sensing by Atg1 and Atg13. Blue arrows represent activation, green arrows represent phosphorylation, blue Ts represent inhibition and gray arrows represent increases in intracellular concentrations.

hypo-phosphorylated upon nutrient starvation (Stephan et al., 2009). Of note, Tor is inactivated upon amino acid starvation (Yuan et al., 2017), which, in addition to PKA would make Atg13 an important sensor for carbon and nitrogen starvation. Although phosphomimetic substitutions in Atg13's tMIM are known to decrease the affinity for Atg1's tMIT (Fujioka et al., 2014), it is still controversial whether the Atg1/Atg13 subcomplex forms exclusively under starvation conditions or whether it is a constitutive complex independent of the cells nutritional state (Fujioka et al., 2014; Kamada et al., 2000; Kraft et al., 2012). Indeed, initial evidence arguing for a constitutive interaction was based on observed coimmunoprecipitation of Atg1 and Atg13 from fed cells (Kraft et al., 2012), but more recent observations argue that Atg13 is readily dephosphorylated during lysis in the absence of phosphatase inhibitors, suggesting that the apparent constitutive interaction was an experimental artifact (Fujioka et al., 2014). Nevertheless, the MIMs of Atg13 contain several Tor-target serine residues within MIM-C and within the flexible loop between MIM-N and MIM-C (Fujioka et al., 2014), suggesting that phosphorylation and dephosphorylation may play a regulatory role in this interaction, whether or not Atg1 and Atg13 are constitutively bound or not. Determining whether the Atg1/Atg13 is dynamic is important as it will allow us to better understand the key autophagy initiation interactions that cells have evolved to regulate, and could highlight key interactions to target therapeutically.

Atg1 kinase activation.

The Atg1 kinase is the most upstream catalytic component of autophagy and is essential to transduce signals in response to cellular stress (Papinski et al., 2014; Reggiori et al., 2004a; Stephan et al., 2009; Yeh et al., 2010). Thus, understanding how this kinase is activated could provide useful insights into how disease and aging affect autophagy (Galluzzi et al., 2015; Gomes and Dikic, 2014; Menzies et al., 2015; Mizushima and Komatsu, 2011). Under fed conditions, Atg1 kinase activity is auto-inhibited through an intrinsic activation loop that blocks the active site (Figure 5a); however, upon starvation, Atg1 auto-activates in an Atg13-dependent manner by phosphorylating its activation loop, resulting in displacement of this loop and exposure of the active site (Kamada et al., 2000; Kijanska et al., 2010; Yeh et al., 2010) (Figure 5b). This Atg1 activation is essential for autophagy progression (Yeh et al., 2010) and Atg1 is known to play critical roles in phosphorylating some autophagy proteins downstream of the phagophore formation process (Papinski et al., 2014). Additionally, Atg1 is reported to phosphorylate two AIC

components (Atg13 and Atg29), which occurs concomitantly with dissociation of the AIC and, presumably a cessation of autophagic initiation (Rao et al., 2016). How these seemingly opposing kinase activities – positive regulation of the downstream components and negative-feedback regulation of the AIC – are temporally regulated to support AIC disassembly is an open area of research. A possible mechanism is that all these protein substrates of Atg1 evolved to have different association constants with Atg1, which favors a specific order of Atg1-mediated phosphorylation.

Mechanistically, this critical Atg1 activation reaction could occur either by auto-phosphorylation *in cis* through direct phosphorylation of one kinase domain's own activation loop, or *in trans,* with one kinase domain phosphorylating the activation loop of a second Atg1 kinase domain. This distinction is important as the *in trans* model necessitates assembly of higher order AICs, and motivates our goal to understand how such Atg1-Atg1 multimers might assemble, disassemble, interact with other autophagy proteins, and respond to cellular stimuli. In support of the *in trans* model, addition of an exogenous dimerization domain to Atg1 increases autophosphorylation in the absence of starvation (Yeh et al., 2011), which suggests that endogenous autophagy proteins could facilitate Atg1 dimerization and transphosphorylation in a nutrient-dependent manner. Indeed, chemical induction of autophagy using the Tor inhibitor rapamycin increases Atg1 self-interaction (Yeh et al., 2011) and activation loop phosphorylation in an Atg13-dependent manner *in vivo* (Kabeya et al., 2005; Yeh et al., 2011). These data suggest that Atg13 is at least partially responsible for bringing two Atg1 molecules in close proximity and allowing for autophosphorylation. Of note, these co-immunoprecipitation (co-IP) studies cannot exclude a model in which Atg13 forms a complex with several Atg1 molecules and induces autophosphorylation of each Atg1 kinase *in cis*. A final observation supporting the *in trans* model is that the isolated Atg1^{EAT} motif is a dimer in

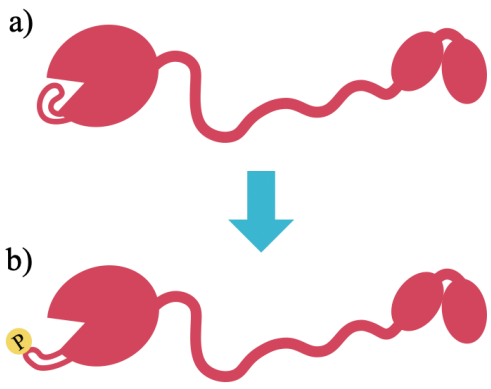

Figure 5: Conformations of inactive and active Atg1 kinase. **a)** Auto-inhibited conformation of Atg1 in which the activation loop is unphosphorylated and blocking the active site. **b)** Active conformation of Atg1 in which the phosphorylated activation loop can no longer block the active site.

solution irrespectively of the presence of Atg13 (Ragusa et al., 2012; Stjepanovic et al., 2014), suggesting that Atg1 might have an intrinsic mechanism for self-assembly that could be facilitated by other AIC components. Nonetheless, full length Atg1 was reported to be monomeric in solution (Rao et al., 2016), suggesting that full-length Atg1 self-interactions may require additional factors.

In addition to Atg13, maximal activation of Atg1 kinase activity requires Atg17, another regulator of the starvation-induced Atg1 kinase activity (Yeh et al., 2010, 2011). While I will detail the structure and known interactions of Atg17 in subsequent chapters, I highlight a few key observations of its role in Atg1 activation here. *In vivo* co-IP experiments (Kabeya et al., 2005) and *in vitro* cross-linking mass spectrometry experiments done on the pentameric AIC (Chew LH et al., 2015) suggest that Atg13 is the only AIC component that directly interacts with Atg1. These observations suggest that Atg17 may contribute to Atg1 kinase activation indirectly. Of note, the described crosslinking experiments could not conclusively exclude direct Atg1-Atg17 interactions as they relied on a truncated version of Atg1 and such co-IP and XL-MS experiments are generally prone to false-negatives. While evidence of a direct Atg1-Atg17 interaction is lacking, it is clear that Atg17 plays some role in activating the kinase. Specifically, knocking out Atg17 reduces Atg1-mediated phosphorylation of myelin basic protein in an *in vitro* phosphorylation assay (Kamada et al., 2000). Interestingly, it was also noted that knocking out Atg17 does not have an effect on Atg1 self-association (Yeh et al., 2011), suggesting that Atg17 contributes to Atg1 kinase activation by a different and unknown mechanism.

Open questions on Atg1/Atg13 complex formation.

An important open question on the formation of the Atg1/Atg13 complex is the true role of the $Atg1^{EAT}$ motif in the overall process (Ragusa et al., 2012). Indeed, as discussed above, its oligomeric state is disputed (Ragusa et al., 2012; Rao et al., 2016) and, as I will discuss in Chapter 4, the $Atg1^{EAT}$ motif was reported to bind and tether high curvature lipid vesicles *in vitro*, which could be important in what is thought to be the key activity of the AIC – recruiting and potentially fusing Atg9-loaded vesicles at the PAS (Ragusa et al., 2012; Rao et al., 2016). Reconciling these apparently contradicting evidence surrounding the oligomeric state(s) of Atg1 at the PAS could provide both important insights into the Atg1 auto-phosphorylation mechanism, and also help us better understand how the pentameric AIC tethers and potentially fuses high-curvature lipid

vesicles to start autophagosome biogenesis. Despite the controversy, henceforth I will assume that full-length Atg1 is monomeric and that the Atg1^{EAT} motif does not tether Atg9-loaded vesicles based on my analysis of the existent data.

A model for Atg1/Atg13 complex formation.

Based on the described data, I propose the following model for the formation of the Atg1/Atg13 (Figure 6): Under fed conditions, Atg1 is phosphorylated at its central IDR by PKA and Atg13 is phosphorylated at its C-terminal IDR by PKA and Tor. In their phosphorylated forms, Atg1/Atg13 complex formation is disfavored (Figure 6a). Upon nutrient starvation, however, the Tor and PKA kinases are inactivated, leading to phosphatase-mediated dephosphorylation of Atg1 and Atg13. According to my model, dephosphorylation of Atg1 and Atg13 then induces conformational changes in these proteins that allow them to bind through a rigid interface in a 1:1 stoichiometry that stabilizes the Atg1^{EAT} motif. In Chapter 3, I will also argue that Atg17 facilitates Atg13 self-interactions that in turn bring two Atg1 molecules into close proximity to allow for transphosphorylation.

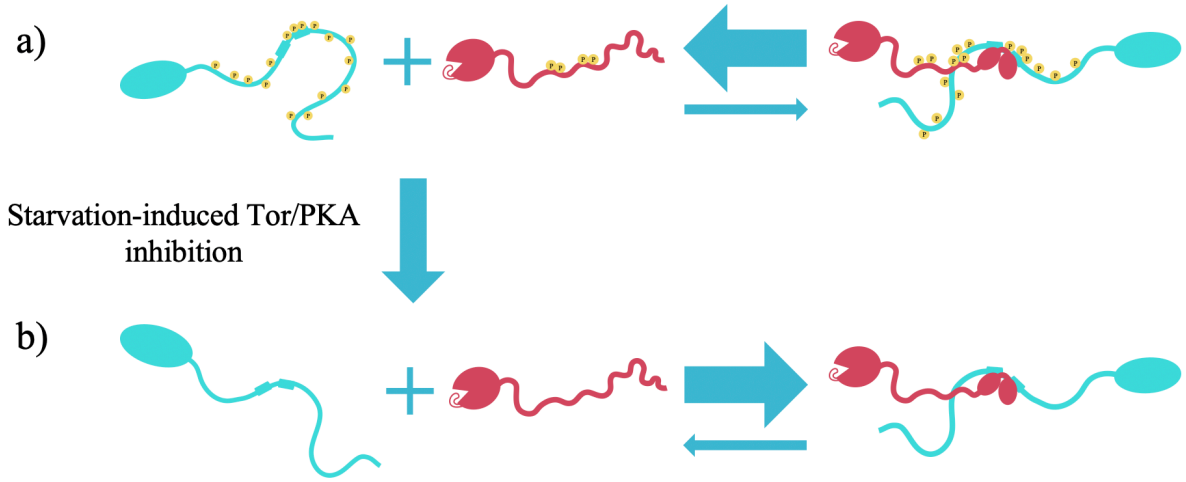

Figure 6: Model for the assembly of the Atg1/Atg13 complex. **a)** Under fed conditions, the IDRs of Atg13 and Atg1 are phosphorylated, which disfavors Atg1/Atg13 complex formation. **b)** The starvation-induced inhibition of Tor and PKAs results in the phosphatase-mediated dephosphorylation of Atg1 and Atg13, allowing the proteins to adopt a conformation that allows them to bind through a rigid interface that stabilizes the Atg1^{EAT} motif. Arrows represent chemical equilibria.

Chapter 2: Interactions between Atg17, Atg29 and Atg31

Upon starvation, the Atg1/Atg13 complex described above is thought to interact with the starvation-specific Atg17/Atg29/Atg31 subcomplex (Kabeya et al., 2009; Kawamata et al., 2008) giving rise to a pentameric AIC (Stjepanovic et al., 2014). As I will discuss in Chapter 4, this pentameric AIC thought to play a crucial role in the starvation-induced recruitment and fusion of Atg9-loaded vesicles required for autophagosome formation (Ragusa et al., 2012; Rao et al., 2016). Despite the known importance of the Atg17/Atg29/Atg31 complex, the mechanism of formation of this subcomplex is poorly understood and is ripe for exploration. In this chapter, I will discuss what is known mechanistically about the formation of the Atg17/Atg29/Atg31 subcomplex and what open questions remain.

Atg17: An AIC organizer.

In addition to facilitating Atg1 activation (Yeh et al., 2010, 2011), Atg17 is thought to be the main organizer of the PAS (Rao et al., 2016; Suzuki et al., 2007), and one of the first proteins to arrive there (Kawamata et al., 2008; Suzuki et al., 2007). In support of this organizational role, genetic epistasis experiments showed that Atg17 was required for rapamycin-dependent PAS localization of Atg1, Atg13 and most of the other early autophagy Atg proteins, but that Atg17 itself could localize to the PAS in the absence of these other components (Table 1a). Importantly, as I will discuss below, the only two exceptions found (Atg29 and Atg31) are thought to form a constitutive complex with Atg17 and arrive at the PAS as a complex (Kabeya et al., 2009; Kawamata et al., 2008). In further support of Atg17's organizational role, quantitative fluorescence

a)

	Atg9-GFP	Atg1-GFP	Atg13-GFP	Atg17-GFP
WT	1.00	1.00	1.00	1.00
atg9-Δ	NA	2.68	5.75	4.62
atg1-Δ	6.07	NA	3.62	25.79
atg13-Δ	4.50	0.69	NA	10.04
atg17-Δ	0.45	0.40	0.39	NA

b)

		Atg17-GFP	Atg29-GFP	Atg31-GFP
atg11-Δ		+	+	+
	atg17-Δ	NA	-	-
	atg29-Δ	-	NA	-
	atg31-Δ	-	-	NA

Table 1: Genetic epistasis experiments suggesting that Atg17 is a central organizer of the AIC. **a)** Relative fluorescence microscopy quantification of the PAS localization of the proteins specified in the columns in the strains specified in the rows. Blue cells indicate combinations in which the PAS localization of the protein specified in the column was disrupted by the genetic ablation of the gene indicated in the row. (Adapted from Suzuki *et al*, 2007). **b)** Qualitative analysis of PAS localization of the proteins specified in the columns in the strains specified in the rows; + indicates PAS localization and - indicates no PAS localization; blue cells indicate combinations in which the PAS localization of the protein specified in the column was disrupted by the genetic ablation of the gene indicated in the row. Of note, experiments in **b)** were carried out in an *atg11-Δ* background to discard effects of non-starvation-induced autophagy (see Lynch-Day and Klionsky, 2010).

microscopy experiments suggest that Atg17 is constitutively present at the PAS (Köfinger et al., 2015), and artificial targeting of Atg17 to the cell membrane by an exogenous transmembrane domain results in other Atg proteins forming a PAS-like structure at the membrane (Suzuki et al., 2007). Furthermore, as I will further discuss in Chapter 4, Atg17 has also been suggested to have an Atg9-binding activity (Rao et al., 2016). Taken together, these observations highlighting the importance of studying Atg17 interactions with other AIC components in understanding autophagy initiation.

Structural studies have shown that Atg17 homodimerizes via a C-terminal helix (Ragusa et al., 2012) (Figure 7) and this dimerization is essential for PAS organization and for autophagy progression (Ragusa et al., 2012; Rao et al., 2016). While Atg17 is generally thought to be a constitutive dimer (Chew et al., 2013; Köfinger et al., 2015; Rao et al., 2016), neither the dimerization kinetic constants nor the dimerization equilibrium constant has been reported, raising the possibility that Atg17 dimers may in fact rapidly exchange with monomers under physiological conditions. As I will discuss in Chapters 3 and 4, Atg13 binds at the Atg17 dimer-dimer interface, and Atg17 dimerization has been suggested to play a role in regulating the Atg9-binding activity of Atg17 (Rao et al., 2016). Thus, figuring out whether the dimers are constitutive could provide important mechanistic insights into how the AIC is assembled and how it recruits and fuses Atg9-loaded vesicles.

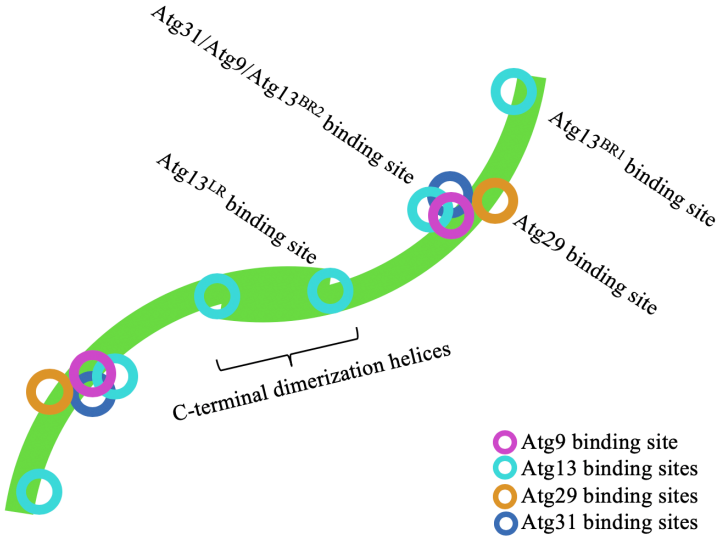

Figure 7: Binding sites for other AIC components on the Atg17 dimer. Schematic of the Atg17 dimer (green) indicating the location of the binding sites for Atg9, Atg13, Atg29 and Atg31. Binding sites shown are based on the crystal structure of the Atg17/Atg29/Atg31 trimeric complex (PDB: 4HPQ), which has been abstracted for simplicity.

As evidenced by crystal structures, Atg17 forms a complex with the Atg29 and Atg31 members of the AIC (Kawamata et al., 2008; Köfinger et al., 2015; Ragusa et al., 2012; Stjepanovic

et al., 2014), which have been suggested to regulate the activity of Atg17 (Rao et al., 2016). While I will further discuss this putative regulation in chapters 3 and 4, here I discuss what is known about the mechanism of assembly of the Atg17/Atg29/Atg31 trimeric complex.

Atg29: A poorly characterized, weakly conserved Atg1 scaffolding component.

As I will discuss in Chapter 4, Atg29 is a putative regulator of Atg17's ability to bind to Atg9 and, like Atg17, Atg29 is required for full starvation-induced autophagic activity (Kawamata et al., 2005; Mao et al., 2013). Atg29 is composed of two distinct regions (Figure 8): a folded N-terminal domain that associates with Atg31 through a beta sandwich formed via strand exchange between the both proteins (Ragusa et al., 2012) (Figure 8), and a large C-terminal region that is predicted to be intrinsically disordered and is thought to somehow regulate autophagy in a phosphorylation-dependent manner (Mao et al., 2013). Specifically, the starvation-induced phosphorylation of the three most C-terminally located serine residues was shown to be essential for full autophagic activity, but neither the responsible kinase(s), nor the mechanistic role of these phosphorylation events was reported (Mao et al., 2013). Of note, at separate study (Rao et al., 2016) reported that Atg1 phosphorylates the C-terminus of Atg29 *in vitro* upon addition of ATP to the pentameric AIC, suggesting that Atg1 is responsible for these key Atg29 phosphorylation events. It remains an open question, however, whether there is another kinase with partial redundancy with Atg1 that may also phosphorylate the C-terminal IDR of Atg29 and thus regulate autophagy progression, and which of the 23 serine residues in the C-terminal IDR of Atg29 (Mao et al., 2013) are important for this regulation. Answering these important questions may not only provide us with a new potential kinase target for small molecule drugs, but also help understand what appears to be an essential step in autophagy progression.

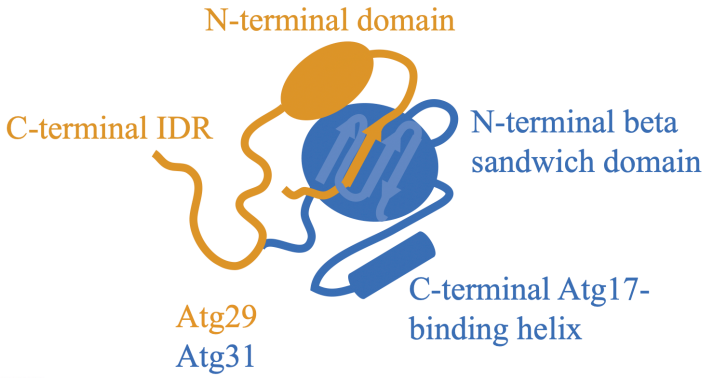

Figure 8: Architecture of the Atg29/Atg31 complex. Schematic of the Atg29/Atg31 dimer based on the crystal of the trimeric Atg17/Atg29/Atg31 complex (PDB: 4HPQ). Atg29 consists of an N-terminal folded domain followed by a putative C-terminal IDR. Atg31 consists of an N-terminal beta sandwich consisting of beta strands from Atg29 and Atg31, and a C-terminal helix that interacts with Atg17.

While a specific mechanistic role of Atg29 phosphorylation in autophagic progression has not yet been elucidated, it is clear that Atg29 phosphorylation is dispensable for formation of the Atg29/Atg31 or the Atg17/Atg29/Atg31 subcomplexes (Mao et al., 2013). Indeed, I and other groups have expressed and purified Atg29/Atg31 in *E. coli* as a complex (Chew et al., 2013; Chew LH et al., 2015; Fujioka et al., 2014; Köfinger et al., 2015; Ragusa et al., 2012; Rao et al., 2016; Stjepanovic et al., 2014), presumably in their unphosphorylated forms, and this dimer can be assembled with Atg17 also produced in *E. coli*, suggesting that Atg29 phosphorylation is dispensable for binding to Atg17. Nevertheless, in Chapter 4, I argue that Atg29 phosphorylation could play a role in the activation of the Atg9-binding activity of Atg17. In the subsequent chapters, I discuss other critical AIC interactions that motivate and provide context for this activation model.

Atg31: A key facilitator of Atg17 and Atg29 association.

The last component of the trimeric complex discussed in this chapter, Atg31, is also necessary for full starvation-induced autophagic activity (Kabeya et al., 2007) and it contains two predicted IDRs that span roughly 50% of the protein (Feng et al., 2015) (Figure 8). Like the Atg13 and Atg29 IDRs, these Atg31 IDRs contain several mapped phosphorylation sites. While the cognate kinases are not-yet-identified, Atg1 has been excluded as these sites are phosphorylated in an Atg1-null background (Feng et al., 2015; Kabeya et al., 2009). In contrast to Atg29, Atg31 is reported to be constitutively phosphorylated *in vivo* (Kabeya et al., 2009), which has been interpreted to imply a structural role for the marks as opposed to a regulatory function. Notably, phosphorylation of serine 174 is essential for full autophagic activity, and introduction of a S174A phospho-null mutant results in aberrant accumulation of Atg9-loaded vesicles at the PAS (Feng et al., 2015). These data suggest that Atg31 phosphorylation plays a role in Atg9 recycling, however, how this mark acts structurally or functionally is unclear (Feng et al., 2015). As detailed for Atg29 above, these Atg31 phosphorylation marks must be dispensable for Atg29/Atg31 and Atg17/Atg29/Atg31 subcomplex assembly as we and others have reconstituted these complexes from components expressed and purified in *E. coli* (Chew et al., 2013; Chew LH et al., 2015; Köfinger et al., 2015; Ragusa et al., 2012; Rao et al., 2016; Stjepanovic et al., 2014), suggesting that pS174 phosphorylation may be required in an autophagy step downstream of Atg17/Atg29/Atg31 assembly. It should be noted that no mass spectrometry data has been reported on these purified complexes, so we cannot discard potential *E. coli* phosphorylation sites. Notably,

Atg31 S174 is located at the Atg17 binding interface, and molecular dynamic simulations suggested that pS174 aids in formation of an additional Atg31 alpha helix that interacts with Atg17 and further stabilizes the complex (Feng et al., 2015). As I will discuss in Chapter 4, the Atg29/Atg31 complex has been suggested to inhibit the Atg9-loaded vesicle binding activity of Atg17 (Rao et al., 2016), raising the possibility that pS174 may be important in Atg17 activation. Furthermore, S174 could be subject to phosphatases and kinases and thus modulate Atg31/Atg17 association and downstream AIC assembly.

Atg29/Atg31: An obligate dimer.

Atg29 and Atg31 assemble as a stable dimeric complex (Rao et al., 2016) and, consistent with an obligate dimer, each protein is highly aggregation prone when expressed in isolation in *E. coli*, but stable when co-expressed (Kabeya et al., 2009; Mao et al., 2013; Rao et al., 2016). This initial observation that Atg29 and Atg31 might help each other fold was substantiated by a crystal structure of the Atg17/Atg29/Atg17 complex from the thermophilic yeast *Lachancea thermotolerans*, which is closely related to *S. cerevisiae* (Ragusa et al., 2012). This structure showed that Atg29 and Atg31 interact via a sandwich beta sheet domain in which one beta sheet uses strands from both Atg29 and Atg31 (Ragusa et al., 2012). While it has not been reported whether these proteins can adopt alternative folds in isolation or if they can exchange with monomers, based on the structural data, I will treat them as an obligate heterodimer for the remainder of this discussion.

Recent epistasis experiments showed that Atg17, Atg29 and Atg31 are mutually essential for their PAS localization upon rapamycin treatment (Kawamata et al., 2008), suggesting that the three proteins arrive at the PAS as a complex (Table 1b). This evidence, together with the suggestion that Atg17 is constitutively present at the PAS (Köfinger et al., 2015), raises the possibility that Atg29 and Atg31 are also constitutively present at the PAS, but this Atg29/Atg31 localization assay has not been directly performed. The genetic data described above recapitulate biochemical observations consistent with a constitutive complex, as whole-cell lysate gel filtration experiments showed that the three proteins form a stable complex independent of the nutritional state of the cell (Kabeya et al., 2009). Nevertheless, no dimerization kinetic or thermodynamic parameters of complex formation have been reported and it remains possible that formation of the

Atg17/Atg29/Atg31 complex could be dynamic and regulated. As I will discuss in Chapter 4, the Atg29/Atg31 dimer has been suggested to compete with Atg13 and Atg9 for binding to Atg17. Testing this model, which could provide us with important clues of how Atg9-loaded vesicles are recruited to the PAS and subsequently fused, will require further understanding of the dynamics of Atg17/Atg29/Atg31 complex formation.

The Atg17/Atg29/Atg31 trimer: a putative vesicle scaffold.

As I will further discuss in Chapter 4, the Atg17/Atg29/Atg31 complex is suggested to act as a vesicle scaffold and to have an important role in the AIC-mediated fusion of Atg9-loaded vesicles (Ragusa et al., 2012; Rao et al., 2016). The crystal structure of the Atg17/Atg29/Atg31 trimeric complex showed that Atg17 adopts an interesting S-shaped double crescent shape (Figure 9) whose radius of curvature is similar to that of Atg9-loaded vesicles (Ragusa et al., 2012). Intrigued by this similarity, the authors suggested that Atg17 may act as a receiving cup for Atg9-loaded vesicles, potentially catalyzing both their recruitment and fusion (Ragusa et al., 2012). Notably, this putative Atg9-vesicle binding site is on the same face of Atg17 that binds to Atg31/Atg29 (Rao et al., 2016) and this model thus suggests that Atg29/Atg31 are negative regulators of Atg9-loaded vesicle recruitment. To accommodate Atg9-vesicle recruitment, this model necessitates either dissociation of Atg31/Atg29 upstream of Atg9-vesicle binding, or a dramatic structural rearrangement of the Atg17/Atg29/Atg31 complex. How this conformational or compositional change might be regulated is completely unexplored and motivates the biochemical experiments described in Chapter 5. Interestingly, negative stain electron micrographs of Atg17 imaged in isolation showed that while the C-terminal dimerization interface is stable, the N-terminus of Atg17 is flexible, which enables the dimer to expand and contract like a spring (Chew LH et al., 2015). In contrast, addition of Atg29/Atg31 stabilizes this spring-like motion and generally rigidifies the complex.

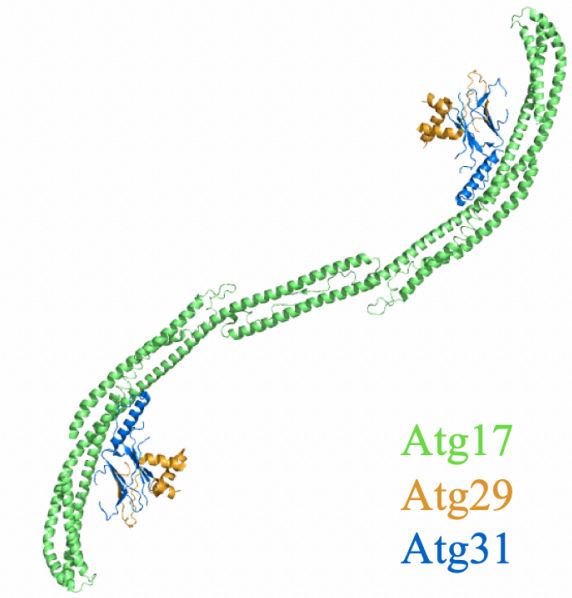

Figure 9: Crystal structure of L. thermotolerans Atg17/Atg29/Atg31 complex. (PDB: 4HPQ).

These data suggest that Atg29 and Atg31 might play a role in stabilizing the rigid S-shape that Atg17 adopts in the trimeric complex (Chew et al., 2013). Despite these structural studies, whether Atg29/Atg31 affect Atg17 dimerization and whether the Atg29/Atg31 'shape lock' is necessary for binding to other AIC components remain open questions.

Outstanding questions and a path forward.

The role of Atg31 phosphorylation in formation of this trimeric complex is entirely unexplored and warrants detailed biochemical investigation. We need to determine basic kinetic and thermodynamic parameters for assembly of this complex in the presence of phospho-null and phospho-mimetic mutants to begin untangling how these modifications might regulate the assembly process.

Another outstanding question in the formation of the Atg17/Atg29/Atg31 dimer of trimers is the allowed binding order(s). It has been shown that Atg17 can dimerize on its own (Chew LH et al., 2015), that pre-made Atg29/Atg31 dimer can bind Atg17 *in vitro* (Rao et al., 2016), and that a monomeric mutant of Atg17 can bind Atg29/Atg31 (Ragusa et al., 2012). These data suggest one possible binding order (Atg29/Atg31 dimer binding Atg17 monomers before Atg17 dimerization). Nonetheless, whether other binding orders are possible and the frequency with which each path is utilized remains an open question. For instance, we do not know whether Atg29/Atg31 dimer can rigidify Atg17 monomers into a curved shape, and whether this curved monomeric Atg17 is capable of dimerizing to give rise to a full double crescent. The current biochemical and biophysical approaches to study the Atg17/Atg29/Atg31 complex have not been able to answer these important questions.

Finally, it remains unclear whether Atg29 directly contacts Atg17. Although the crystal structure of the trimeric Atg17/Atg29/Atg31 complex suggests that the folded domain of Atg29 lacks direct contacts with Atg17 (Ragusa et al., 2012), this structure could not resolve Atg29's C-terminal IDR, and could not exclude contacts between Atg29 and Atg17. In fact, Atg29 can co-immunoprecipitate Atg17 in an *E. coli* host, and crosslinking-mass spectrometry experiments done on the pentameric Atg1complex implied that the C-terminal tail of Atg29 binds to the concave face of Atg17 (Chew LH et al., 2015). Although it is unknown whether this putative Atg17/Atg29

interaction also occurs in the isolated tetrameric Atg17/Atg29/Atg31 complex, the fact that this putative interaction between Atg17 and Atg29 seems to be mediated by the part of Atg29 that becomes phosphorylated upon starvation (Mao et al., 2013) suggests a new potential *in vivo*-regulated step in autophagy initiation. I propose that tight binding of Atg29/Atg31 to Atg17 is driven by multiple dynamic interactions between Atg31 and Atg29 with Atg17. This way, cells can simultaneously have very tight binding between Atg17 and the Atg29/Atg31 dimer while allowing for easy access of kinases and phosphatases that may regulate this complex. In Chapter 4, I will discuss a model that I propose in which Atg1-mediated phosphorylation of the C-terminal IDR of Atg29 reduces the binding affinity of the Atg29/Atg31 dimer, helping to displace the Atg29/Atg31 dimer from the Atg9 binding site on Atg17 and thus activate the Atg9-loaded vesicle binding activity of the AIC.

A model for Atg17/Atg29/Atg31 assembly.

Based on the data described above, I propose the following model for Atg17/Atg29/Atg31 formation (Figure 10): Atg17, Atg29 and Atg31 are present at the PAS constitutively and they are in a dynamic equilibrium. Atg17 exchanges between monomers and dimers (Figure 10a) while constitutive Atg29/Atg31 dimers quickly alternate between several binding sites for Atg17 (Figure 10b) without affecting the Atg17 monomer-dimer equilibrium. Notably, although this dynamic equilibrium model for the binding of the Atg29/Atg31 dimer to Atg17 implies the existance of a population of dissociated Atg29/Atg31 dimer, I propose that the equilibrium strongly favors the trimeric Atg17/Atg29/Atg31 complex and that the population of unbound Atg29/Atg31 is negligible. For this reason, I will treat Atg17/Atg29/Atg31 as a constitutive complex in the subsequent chapters. Finally, as I will discuss in Chapter 3, I propose that the starvation-induced binding of Atg13 at the Atg17 dimer interface (Fujioka et al., 2014) stabilizes the Atg17 dimer (Figure 10c) which, as I will discuss in Chapter 4, may be important for the putative Atg9-vesicle fusion activity of the AIC.

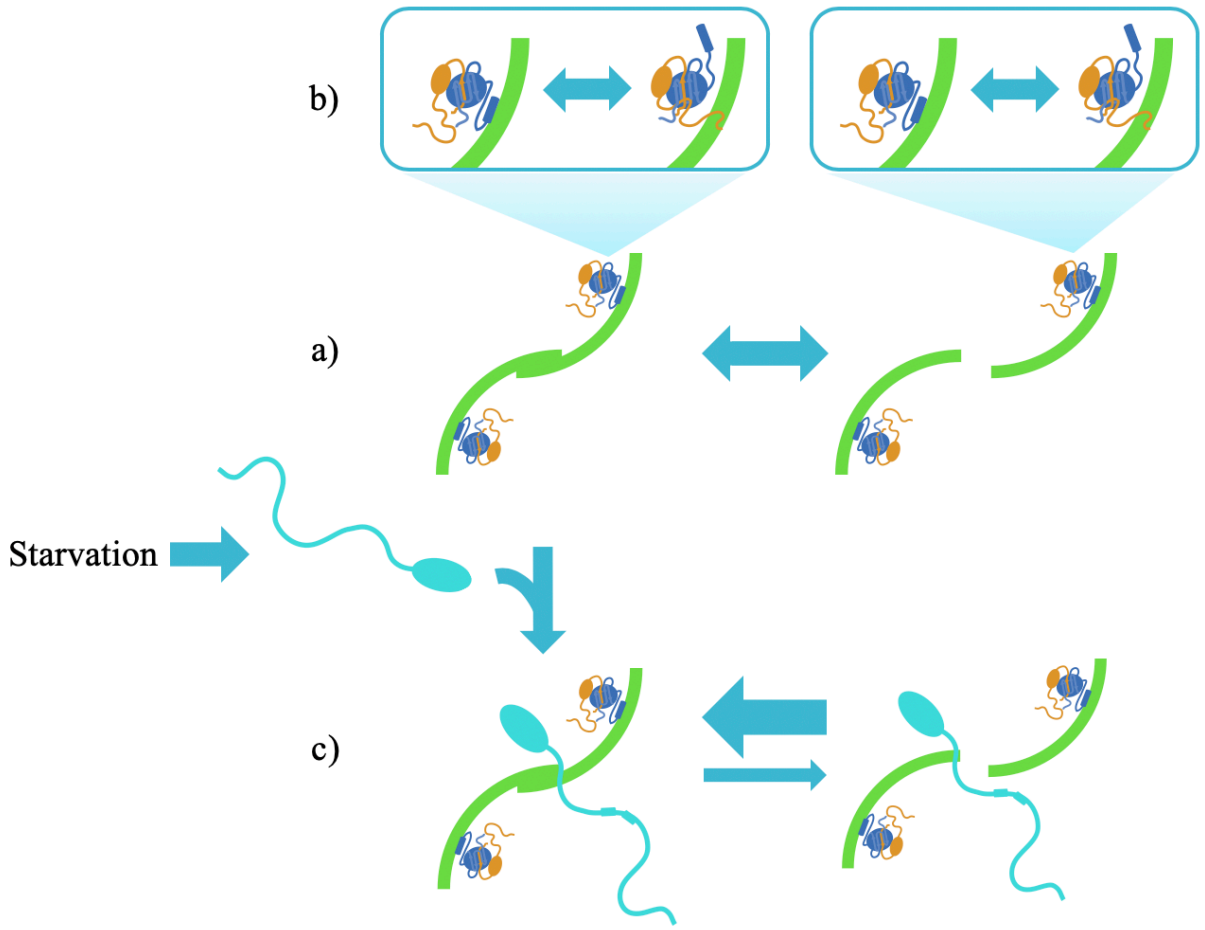

Figure 10: A model for Atg17/Atg29/Atg31 complex formation. Atg17, Atg29 and Atg31 are in a dynamic equilibrium: **a)** Atg17 exchanges between monomers and dimers and **b)** the constitutive Atg29/Atg31 dimers quickly alternate between several binding sites for Atg17 without affecting the Atg17 monomer-dimer equilibrium. Of note, I propose that there is a small population of dissociated Atg29/Atg31 dimer, but that the equilibrium strongly favors the trimeric complex and this population is thus negligible. **c)** Upon starvation, Atg13 binds to the Atg17 dimer interface, stabilizing the Atg17 dimer and thus driving the Atg17 monomer-dimer equilibrium towards the dimeric form.

Chapter 3: Assembly of the pentameric AIC

In the previous chapters, I discussed the isolated assembly of the Atg1/Atg13 and Atg17/Atg29/Atg31 subcomplexes, but these two subcomplexes must come together to produce an active AIC able to recruit Atg9-loaded vesicles (Rao et al., 2016), phosphorylate and regulate downstream autophagy components, and, possibly, catalyze Atg9-vesicle fusion to initiate formation of the phagophore. This AIC assembly process is an essential step for autophagy and is thought to be a critical decision point, effectively committing the cell to undergo starvation-induced autophagy (Kabeya et al., 2005; Kamada et al., 2000; Stephan et al., 2009; Yamamoto et al., 2016). Thus, a deep mechanistic understanding of AIC formation is important for understanding cellular regulation of this potentially destructive pathway and will be vital in the development of therapeutics that regulate autophagy. In this chapter, I discuss our current mechanistic understanding of the formation and activation of the pentameric AIC.

Atg13 is a key protein in the formation and activation of the pentameric AIC.

Atg13 is a crucial protein in the assembly of the complete and active AIC. First, it is the physical link between Atg1 and the Atg17/Atg29/Atg31 complex (Fujioka et al., 2014; Köfinger et al., 2015; Stjepanovic et al., 2014) as no direct contacts have been mapped between Atg1 and any of the Atg17/Atg29/Atg31 components. Second, through an unknown mechanism, Atg13 increases the binding affinity of Atg17 for Atg9 (Rao et al., 2016), which is an essential step in phagophore formation. Finally, Atg13 is thought to crosslink multiple pentameric AICs into higher order oligomers (Yamamoto et al., 2016) and thereby locally concentrates AIC components, which may be crucial for AIC assembly and Atg9-vesicle fusion. Below, I discuss each of these important Atg13 functions separately before discussing a model for pentameric AIC formation.

Atg13 physically links the components of the pentameric AIC.

As discussed in Chapter 1, although both Atg13 and Atg17 (Kabeya et al., 2005; Kamada et al., 2000) are required for Atg1 kinase activation, only Atg13 is thought to directly contact Atg1 (Chew LH et al., 2015). Atg17 and Atg1 are instead thought to be linked through Atg13, as short regions in Atg13's C-terminal IDR are known to bind Atg17 (Fujioka et al., 2014; Yamamoto et al., 2016). This suggests that the important interactions between Atg1 and the Atg17/Atg29/Atg31

complex, such as Atg29 phosphorylation (Mao et al., 2013; Rao et al., 2016), are driven by binding of Atg13 and facilitated by the intrinsic flexibility of this important linker protein. Similar to the regulated Atg1:Atg13 binding discussed in Chapter 1 (Fujioka et al., 2014), this Atg13 linking activity is likely regulated as the Atg17 binding regions on Atg13 contain putative Tor phosphorylation sites that are phosphorylated under basal conditions and become dephosphorylated upon rapamycin treatment (Chew LH et al., 2015; Fujioka et al., 2014; Yamamoto et al., 2016). Consistent with these sites acting as nutrient sensors, phospho-mimetic and phospho-null substitutions affect Atg13/Atg17 binding affinity as expected: phospho-mimetic substitutions generally decrease the K_D and phospho-null substitutions generally increase the K_D (Chew LH et al., 2015; Fujioka et al., 2014; Yamamoto et al., 2016). As I discuss below, Atg13 binding to Atg17 is also thought to play an essential role in activating the AIC's ability to recruit Atg9-loaded vesicles (Rao et al., 2016), which further highlights the importance of tightly regulating these interactions to limit spurious autophagy initiation.

Atg13 mediates the supramolecular assembly of AICs.

In addition to linking Atg1 with the Atg17/Atg29/Atg31 complex, Atg13 may crosslink AICs by simultaneously binding to multiple Atg17 molecules (Yamamoto et al., 2016). Mutational analysis showed that Atg13's C-terminal IDR includes at least two Atg17 binding regions – named 17BR1 (for Atg17 binding region 1) and 17LR (for Atg17-linking region) (Yamamoto et al., 2016) (Figure 11). Of note, the Atg13^{17LR} motif binds Atg17 in hydrophobic pocket at the Atg17 dimer interface (Yamamoto et al., 2016), suggesting that Atg13:Atg17 association could also modulate the Atg17 monomer-dimer equilibrium (see Chapter 2), with dimers favored upon Atg13 binding. Additionally, the observed 17LR binding site suggests that Atg17 dimerization is essential for the supramolecular assembly of AICs, which might explain why C-terminally truncated monomeric Atg17 mutants cannot support starvation-induced autophagy (Ragusa

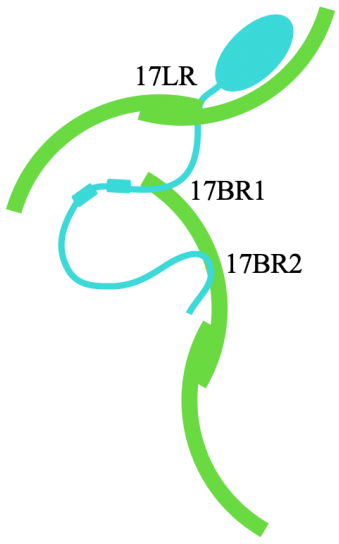

Figure 11: Atg13 crosslinks AICs. Atg13 binds crosslinks Atg17 dimers through at least 2 Atg17 binding sites on Atg13. Atg17 binding sites are named on diagram. Atg1, Atg29 and Atg31 were omitted for clarity.

et al., 2012). Testing and validation of this model will require measuring thermodynamic and kinetic parameters of Atg17 dimerization and analyzing how the binding of other AIC components affects them. Such a detailed understanding of these interactions is important as Atg17 dimerization is necessary for the Atg9-loaded vesicle binding activity of the pentameric AIC *in vitro* (Rao et al., 2016), suggesting that Atg13-mediated stabilization of the Atg17 dimer could be a crucial step leading to Atg9-loaded vesicle fusion *in vivo*.

In addition to the two Atg17 binding sites on Atg13 mentioned above, a third Atg17 binding site has been reported, called 17BR2 (Chew LH et al., 2015) (Figure 11). This binding site appears to be dispensable for the supramolecular assembly of AICs and it is weaker than the other two Atg17 binding motifs on Atg13 (Yamamoto et al., 2016). Nevertheless, as I will further discuss in Chapter 4, $Atg13^{17BR2}$ might play a crucial role in activating the AIC's Atg9-vesicle binding activity.

A proposed role of liquid-liquid phase separation in AIC formation and activation.

Using isothermal titration calorimetry (ITC), the Hurley group (Stjepanovic et al., 2014) measured a ~10 μM K_D for binding between the preformed $Atg1^{tMIM}$/$Atg13^{tMIT}$ and Atg17/Atg29/Atg31 subcomplexes: $2(\text{Atg1:Atg13}) + 2(\text{Atg17:Atg29:Atg31}) \leftrightarrow 2(\text{Atg1:Atg13:Atg17:Atg29:Atg31})$. Given the extremely low intracellular concentrations of these proteins (~1-100 nM) (Belle et al., 2003), this relatively weak binding affinity is surprising and implies that the Atg1/Atg13/Atg17/Atg29/Atg31 components must be localized and concentrated at the PAS or exist in a tighter binding form (through post-translational modification, for example) to assemble as an active pentameric AIC *in vivo*. Based on recent preliminary experiments performed by Samantha Webster (personal communication), I will argue that the local concentrations of AIC components are increased via liquid-liquid phase separation and that the PAS is a dynamic, phase-separated condensate of Atg proteins.

Liquid-liquid phase separation (LLPS) is a reversible, dynamic protein assembly phenomenon whereby multivalent interactions between intrinsically disordered proteins separate and concentrate intracellular components in a droplet-like condensate (Boeynaems et al., 2018; Li et al., 2012). All these requirements are fulfilled by the components of the AIC. First, Atg1, Atg9,

Atg13, Atg29 and Atg31 have long predicted intrinsically disordered regions (Feng et al., 2015; Mao et al., 2013; Meia et al., 2014; Yamamoto et al., 2016). Second, as discussed above, Atg13 interacts with Atg1 and Atg17 via multivalent interactions (Yamamoto et al., 2016) and there are likely additional as-yet-uncharacterized interactions between the poorly characterized IDRs of other AIC components. Finally, gel filtration experiments showed that upon dilution, the AIC dissociates into subcomplexes, demonstrating that the AIC assembly is reversible (Yamamoto et al., 2016). For all these reasons, I propose that PAS is a phase-separated condensate that increases the local concentrations of the AIC components and facilitates the formation of the aforementioned ordered contacts in the pentameric AIC. Further, I propose that this behavior is regulated by the starvation-induced dephosphorylation of Atg13 (Stephan et al., 2009) and that by increasing the local concentration of Atg1 at the PAS, LLPS also helps to bring Atg1 kinases in close proximity, allowing for trans-phosphorylation and activation of Atg1 kinase (Figure 12a-h) activity. In Chapter 1, I discussed that Atg13 was essential for the self-assembly and auto-phosphorylation of Atg1 (Yeh et al., 2010, 2011). Based on the LLPS model described above, I propose that upon starvation, dephosphorylation of Atg13 induces not only the formation of the Atg1/Atg13 complex, but also the LLPS of the IDRs of Atg13, Atg1, Atg31 and Atg29 at the PAS. According to my model, this LLPS increases the local concentration of both the Atg1/Atg13 and the Atg17/Atg29/Atg31 complexes at the PAS, which facilitates pentameric AIC formation.

Atg1 phosphorylation causes the dissociation of the AIC.

Above, I have focused on the regulated, rapid assembly of the pentameric AIC, which enables autophagic degradation. Clearly, it is also vital that cells can inhibit this pathway to rapidly stop degrading cytoplasmic components once nutrients become available. Given the putative role of the AIC in cellular decision making discussed in the previous chapters, disassembly of the AIC seems a likely place to downregulate autophagic flux upon nutrient availability. Thus, understanding the disassembly of the AIC is also of great importance. As discussed, nutrient-induced activation of Tor and the subsequent phosphorylation of Atg13 drives dissociation of Atg13 from Atg17/Atg29/Atg31 (Chang and Neufeld, 2009; Kamada et al., 2000; Kaur and Debnath, 2015; Stephan et al., 2009; Thevelein et al., 2000). Additionally, *in vitro* studies showed that the addition of ATP to a pentameric AIC assembled from purified components results in Atg1-mediated phosphorylation of Atg13 and Atg29 and the concomitant dissociation of the pentameric

AIC into Atg1/Atg13 and Atg17/Atg29/Atg31 subcomplexes (Rao et al., 2016), suggesting that the active Atg1 kinase could negatively feedback on AIC formation. Interestingly, several of the Atg1 phosphorylation sites on Atg13 are serine residues that become dephosphorylated upon rapamycin treatment and map to the tMIM, 17BR1 and 17BR2 motifs of Atg13 (Rao et al., 2016), which are binding sites for Atg1 and Atg17. This apparent partial redundancy of Atg1 and Tor could be beneficial to the cell, as the effective concentration of Atg1 in the pentameric AIC is likely much higher than that of cytosolic Tor, and high local Atg1 concentrations could allow for faster phosphorylation and dissociation of the AIC upon nutrient addition. Moreover, these data also suggest that constant autophagic flux would require continuous signaling and continuous assembly of AIC, which would allow the cell to rapidly stop starvation-induced autophagy once it is no longer needed, consistent with the AIC disassembling within 10 minutes of nutrient re-addition *in vivo* (Kawamata et al., 2008). While both the activatory and inhibitory roles of Atg1 have been reported, it remains unclear how the cell balances and regulates these disparate functions.

The role of Atg1-mediated phosphorylation of Atg29 on AIC disassembly is unknown. Nonetheless, knocking out the Atg1 kinase activity results in the aberrant accumulation of Atg29 at the PAS, suggesting that Atg29 phosphorylation might play a role in the shuttling Atg29 from the PAS to the cytoplasm (Kawamata et al., 2008). Notably, most of the Atg1 phosphorylation sites on Atg29 are in its C-terminal IDR (Rao et al., 2016), a region of Atg29 that is phosphorylated upon nutrient deprivation and whose phosphorylation was shown to be essential for starvation-induced autophagic activity (Mao et al., 2013). I propose that Atg1 phosphorylates the C-terminal IDR of Atg29 in the context of an assembled AIC and that this modification decreases the binding affinity of the Atg29/Atg31 dimer for Atg17. According to my model, phosphorylation-mediated dissociation of the Atg29/Atg31 dimer could then activate Atg17 for Atg9-loaded vesicle binding. In support of my model, three of the Atg1 phosphorylation sites on the C-terminal tail of Atg29 map to a region of Atg29 that was shown by XL-MS to crosslink to the convex face of Atg17 in the context of the pentameric AIC (Chew LH et al., 2015; Rao et al., 2016).

The evidence described above suggests that there is exquisite regulation of AIC disassembly, which could be a likely place for disease mutations to act. Thus, understanding the

cellular factors that mediate the dismantling of the AIC have great potential to help us understand how autophagy may fail in various proteostasis-related diseases and aging (Galluzzi et al., 2015; Gomes and Dikic, 2014; Menzies et al., 2015; Mizushima and Komatsu, 2011).

A model for pentameric AIC assembly.

Based on the evidence discussed in this chapter, I propose the following mechanism for the formation of the pentameric AIC (Figure 12): Atg17/Atg29/Atg31 form a stable, trimeric complex that is constitutively present at the PAS (Kabeya et al., 2009; Kawamata et al., 2008), and these trimers are in dynamic equilibria with higher-order complexes through Atg17-mediated dimerization (Figure 12a). In my model, the Atg29/Atg31 dimer is stably bound to Atg17 via multiple exchanging interactions between Atg29/Atg31 and Atg17 dimer (Figure 12b), and this binding of Atg29/Atg31 to Atg17 stabilizes a high-curvature conformation of Atg17 (Chew et al., 2013), which also stabilizes the tightest binding site for Atg13 on Atg17 (Chew et al., 2013; Fujioka et al., 2014). Upon starvation, Atg13 is dephosphorylated at several sites including the binding sites for Atg1 and Atg17 (Fujioka et al., 2014; Yamamoto et al., 2016) and Atg1 is also dephosphorylated at its central IDR (Figure 12c). Dephosphorylation of Atg1 and Atg13 results in the formation of the Atg1/Atg13 complex (Figure 12d) and also allows Atg13 to undergo liquid-liquid phase separation (LLPS) with the IDRs of Atg29 and Atg31 (Figure 12e). This LLPS increases the local concentrations of the Atg1/Atg13 and Atg17/Atg29/Atg31 subcomplexes above the K_D for the interaction between these two subcomplexes, thus driving pentameric AIC formation through Atg13/Atg17 binding (Figure 12f). Additionally, in my model, a high order AIC is formed when Atg13 binds to Atg17 using two different binding sites on different Atg17 molecules (17LR and 17BR1, see figure 11), effectively crosslinking AICs (Figure 12g). This supramolecular assembly of AICs brings Atg1 molecules in close proximity with one another (Figure 12g inset), allowing for transphosphorylation and Atg1 kinase activation (Figure 12h). Once Atg1 is activated, it phosphorylates the C-terminal IDR of Atg29 (Figure 12i), causing a decrease in the binding affinity of Atg29 for Atg17, disrupting the avidity effects and thus reducing the overall binding affinity of Atg29/Atg31 for Atg17 (Figure 12i inset). The reduced affinity of Atg29/Atg31 for Atg17 allows the third Atg17 binding motif on Atg13 (17BR2, see figure 11), whose effective concentration for Atg17 is now very high, to displace the Atg29/Atg31 dimer from Atg17 face and thereby uncover the Atg9-binding site on Atg17 (Figure 12j, further discussed in Chapter 4). In

the model I propose, the dissociated Atg29/Atg31 dimer stays at the PAS in a LLPS state via linkages to Atg13 and other AIC components with IDRs until i) the binding site for Atg31 on Atg17 is no longer occupied by either Atg9 or Atg13 and ii) the C-terminal IDR of Atg29 becomes dephosphorylated, allowing Atg29/Atg31 to re-bind Atg17 using the canonical motifs described above. Eventually, the active Atg1 kinase phosphorylates Atg13 at the three Atg17 binding sites, leading to disassembly of the pentameric AIC into Atg1/Atg13 and Atg17/Atg29/Atg31 subcomplexes. Further phosphorylation of Atg13 causes disruption of the IDR-based contacts required for LLPS and the subsequent dissolution of the condensate (Figure 12k). At this point, if the cell is still starved, Tor will be deactivated and Atg13 will become dephosphorylated at the Atg17 binding sites, repeating the whole process (Figure 12l). On the other hand, if the cell is no longer starved, Tor re-activation will further phosphorylate Atg13 at the Atg1 binding site, further dissociating the Atg1/Atg13 complex and causing the cessation of further autophagy initiation (Figure 12m).

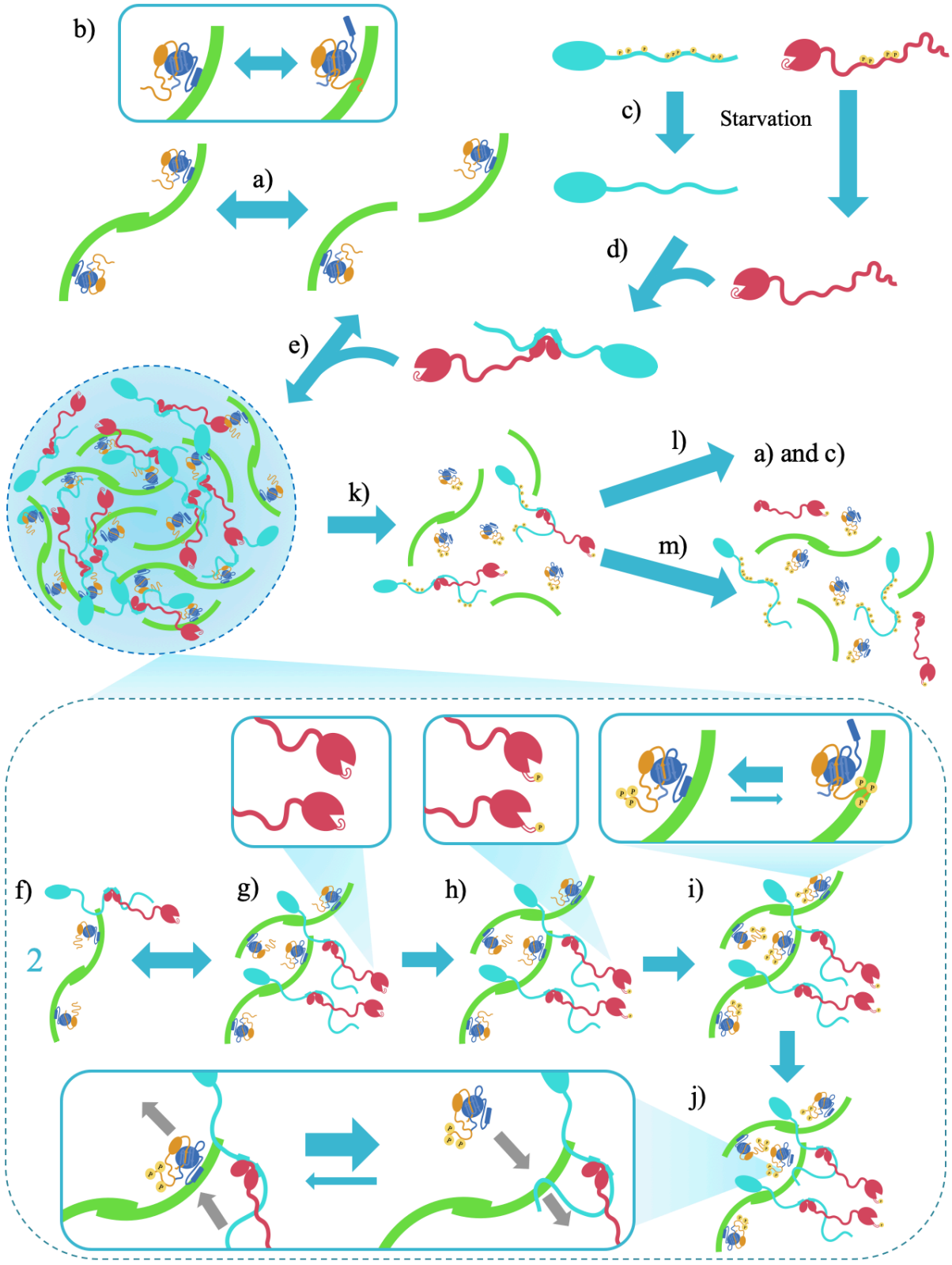

Figure 12: A model for the assembly of the pentameric AIC. Blue arrows indicate reaction equilibria, gray arrows indicate binding mechanisms (see main text for full step-by-step description).

Assembly of the pentameric AIC: open questions and future directions.

As discussed, the highly flexible Atg13 contains several characterized phospho-regulated binding sites for Atg1 and Atg17 in addition to several uncharacterized ones (Fujioka et al., 2014; Stephan et al., 2009). Although many of these phospho-regulated sites have been mapped (Fujioka et al., 2014), it is unknown whether these dephosphorylation events are sequentially ordered and coupled to local conformational changes required for AIC formation or if these events can occur at random. Likewise, it is unknown whether there is a specific order in the phosphorylation events that is required *in vivo* for efficient complex dissociation. To understand this regulation, both *in vitro* and *in vivo* studies using phospho-mimetic and phospho-null substitutions will be valuable. Additionally, work to identify the cellular phosphatases responsible for these events could provide valuable insights into how cells commit to starvation-induced autophagy, and such enzymes could serve as valuable therapeutic targets (Galluzzi et al., 2015; Gomes and Dikic, 2014; Menzies et al., 2015; Mizushima and Komatsu, 2011). Potential experimental approaches to identify these phosphatases include using phosphatase:substrate complex stabilizing techniques (crosslinking agents or substrate-trapping catalytically-inactive phosphatases mutants) followed by coIP-mass spectrometry (Fahs et al., 2016; Flint et al., 1997; Trakselis et al., 2005).

A second important goal is determining the set of protein stoichiometries allowed stoichiometries in the assembling and assembled AIC. Based on *in vivo* quantitative fluorescence microscopy, Köfinger *et al* proposed that the PAS has a defined number of each AIC component (~30-60 copies of each protein) (Köfinger et al., 2015). Köfinger *et al* also suggested that the AIC is a tetramer of pentamers based on molecular dynamic simulations of small angle X-ray scattering data (SAXS). Nonetheless, the Atg13 construct they used did not include the $Atg13^{17LR}$ motif, which, as discussed above, is critical for the supramolecular assembly of AICs (Köfinger et al., 2015; Yamamoto et al., 2016). Answering questions surround functional AIC stoichiometries is important as it will allow us to better understand which AIC components are limiting in AIC formation, which could in turn help us understand how cells regulate AIC formation. In addition, understanding allowed AIC stoichiometries will help us build better models for the pentameric AIC, which may in turn help us better understand how the AIC carries out its functions.

A third important question in the assembly of the AIC is the allowed binding order(s) of the constituents. Given the number of components of the AIC and the different oligomeric states of these complexes, it is plausible that several binding orders are allowed, as has been observed in bacterial ribosomal assembly (Davis et al., 2016). Allowing for different assembly pathways to occur simultaneously would allow the cell to more quickly assemble and disassemble the AIC at the PAS and thus to mire tightly regulate autophagy. Although in the model above I discussed one possible binding order, I believe that more than one binding order may be possible and that understanding all these possible pathways may in turn help us better select interactions to target with therapeutic agents.

Finally, it remains unclear whether the 17BR2 motif on Atg13 (Chew LH et al., 2015) binds to the same molecule of Atg17 as the 17BR1, or if it links the Atg17/Atg13/Atg17 complex to a third Atg17 molecule. Answering this question could provide us with useful insights into how the AIC forms. First, the number of amino acids between the three Atg17 binding sites on Atg13 is different(Yamamoto et al., 2016). Thus, the three binding sites potentially crosslinking these Atg17 molecules could also provide different gap distances between each Atg17 molecule. This gap spacing could be important in allowing or sterically occluding binding of Atg9-loaded vesicles, and could influence the ability of Atg17 to catalyze their subsequent fusion. For instance, Atg13 could initially crosslink two Atg17/Atg9-loaded vesicle complexes using its two farthest apart Atg17 binding sites, with the distance between the two Atg9-loaded vesicles being insufficient allow for fusion (Figure 13a). Once initially bound, Atg13 could then transfer one Atg17/Atg9 complex to a closer binding site (Figure 13b), bringing the two Atg9-loaded vesicles closer together and facilitating their fusion (Figure 13c). Clearly, further studies are required to test many various permutations of this model. Lastly, although the number of molecules of each AIC member at the PAS upon rapamycin treatment was previously estimated (Köfinger et al., 2015), knowing how many Atg17 molecules can be crosslinked by an Atg13 molecule can help build models for the supramolecular assembly of AICs at the PAS, which might provide us with useful insights into the how the AIC catalyzes Atg9-loaded vesicle fusion.

A unifying factor of the open questions discussed above is that each of them may have several answers, suggesting that AIC complex formation is not a linear pathway, but rather, a

network of interconnected binding reactions. Given this potential heterogeneity in AIC formation and the potential differences in the abundance of some of the individual pathways, genetic and bulk biochemical approaches likely hide many crucial mechanistic insights of AIC formation. This fact motivated a new single-molecule experimental approach that I will discuss in Chapter 5.

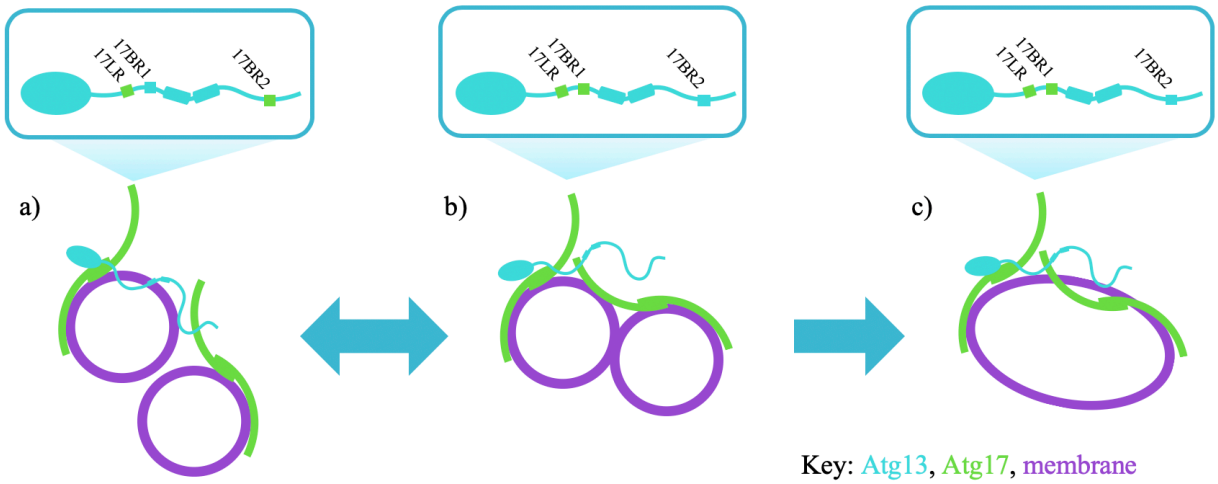

***Figure 13: A model for a potential Atg13-mediated control of Atg-9-loaded vesicle gap distancing and fusion*. a)** Atg13 could initially crosslink two Atg17/Atg9-vesicle complexes using its two farthest apart Atg17 binding sites, with the distance between the two Atg9-loaded vesicles being insufficient allow for fusion. **b)** Once initially bound, Atg13 could then transfer one Atg17/Atg9-vesicle complex to a closer binding site, **c)** bringing the two Atg9-loaded vesicles closer together and facilitating their fusion. Insets highlights in green the Atg17 binding motifs being used in each case. Atg1, Atg29, Atg31 and Atg9 are omitted for clarity.

Once the pentameric AIC is assembled, it recruits Atg9-loaded vesicles to the PAS and is thought to catalyze their fusion to begin phagophore biogenesis(Rao et al., 2016). In the following chapter, I will discuss what is known about how the AIC's recruits Atg9-loaded vesicles to the PAS and propose a mechanism by which the AIC might fuse Atg9-loaded vesicles.

Chapter 4: interactions between the pentameric the AIC and Atg9-loaded vesicles

Once the active pentameric AIC assembles, it recruits high curvature lipid vesicles and is thought to catalyze their fusion to initiate the formation of the phagophore (Rao et al., 2016). These vesicles are loaded with Atg9, the only transmembrane protein essential for autophagy (Noda et al., 2000; Yamamoto et al., 2012), and these high curvature vesicles, which are absolutely required for both selective and non-selective autophagy (Noda et al., 2000), are thought to play a crucial role in facilitating the initial formation of the phagophore (Yamamoto et al., 2012). Interestingly, Atg9-loaded vesicles are not thought to be the main membrane source for autophagosome formation, as evidence suggests only three such vesicles are required for one round of autophagosome formation (Yamamoto et al., 2012). In this chapter, I discuss what is currently known about recruitment of Atg9-loaded vesicles to the PAS and their subsequent fusion.

Atg9: a transmembrane protein essential for initial phagophore formation.

Architecturally, Atg9 consists of six transmembrane helices flanked by long, putatively intrinsically disordered regions at the at the N- and C- termini and an additional small folded domain between helices 2 and 3 (residues 595-543) (Rao et al., 2016; Suzuki et al., 2015) (Figure 14). In the cell, Atg9 resides in high curvature single-membrane vesicles of 30-60nm in diameter, each containing ~27 Atg9 molecules oriented with both terminal IDRs facing the cytoplasm (Yamamoto et al., 2012). These vesicles are thought to be mostly monomeric under fed conditions (Yamamoto et al., 2012) but, as I discus below, starvation induces their higher-order assembly, which is essential for phagophore formation (He et al., 2008). Of note, protein-free vesicles of this size are able to undergo spontaneous fusion *in vitro* (François-Martin et al., 2017), whereas Atg9-loaded vesicles seem to be more stable (Noda et al., 2000; Rao et al.,

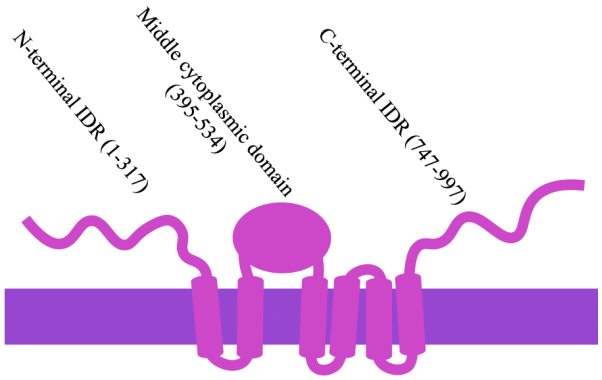

Figure 14: Architecture of S. cerevisiae Atg9. Atg9 consists of a six-pass transmembrane region with a soluble cytoplasmic domain between helices 2 and 3, flanked at the N- and C-termini by long putative IDRs.

2016; Yamamoto et al., 2012), suggesting a vesicle stabilizing role for Atg9. How Atg9 might stabilize these vesicles mechanistically has not been explored. Nonetheless, based on the observed Atg9 trans-vesicle dimerization (He et al., 2008), I propose that when two Atg9-loaded vesicles are in close proximity, Atg9 dimerization ensures that the vesicle's lipids remain sufficiently separated to block spontaneous fusion (Figure 15). My model also predicts that Atg9 packing around the vesicle must be dynamic, exposing Atg9-free regions of the lipid vesicles for fusion upon autophagic induction. As I will discuss in the following sections, Atg9-loaded vesicles interact with several members of the AIC (Feng et al., 2016; Rao et al., 2016; Sekito et al., 2009), which may help to change the distribution of Atg9 molecules within the vesicles, thereby catalyzing vesicle fusion and giving rise to the nascent autophagosome. I will further discuss this model at the end of this chapter.

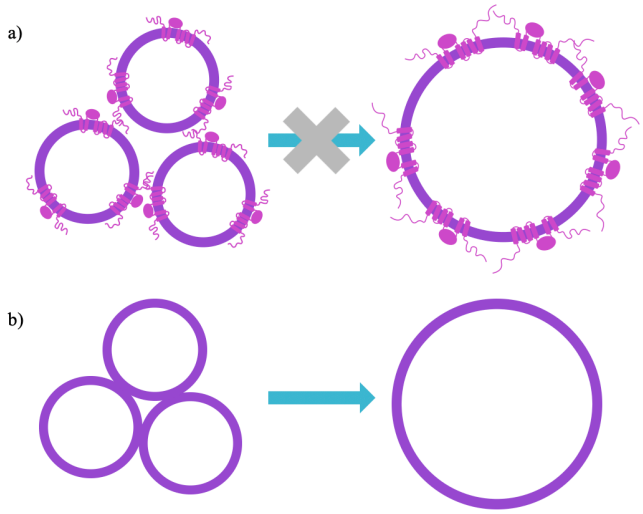

Figure 15: Atg9 oligomerization may block spontaneous lipid vesicle fusion. **a)** In proteoliposomes, Atg9-mediated protein-protein interactions may prevent the vesicles' lipid components from directly contacting one another to spontaneously fuse. **b)** In the absence of Atg9, high curvature vesicles can form direct lipid contacts and spontaneously fuse.

Although Atg9-loaded vesicles are highly dynamic and constitutively cycle between the cytoplasm and the PAS on a ~90-minute timescale (Reggiori et al., 2004a), starvation triggers the AIC-mediated recruitment of Atg9-loaded vesicles to the PAS (Sekito et al., 2009). Below, I describe what is known about how the AIC recruits and catalyzes the fusion of Atg9-loaded vesicles.

The HORMA domain of Atg13 is a strong recruiter of Atg9 to the PAS.

Atg9 and the isolated HORMA domain of Atg13 co-immunoprecipitate in the absence of Atg1, Atg11 and Atg17 (Suzuki et al., 2015), suggesting that Atg9-loaded vesicles could be recruited to the PAS either directly by the HORMA domain or through another subunit mediating this interaction. Consistently, mutational analysis showed that the Atg9/Atg13^{HORMA} interaction is

essential for the recruitment of Atg9 to the PAS (Suzuki et al., 2015). Interestingly, no starvation-induced phosphorylation sites have been found on the HORMA domain of Atg13 (Fujioka et al., 2014), so it is unknown how this interaction can also sense the nutritional status of the cell. Based on observation of other HORMA domains, which can adopt two conformations, Jao *et al.* (Jao et al., 2013) proposed a model in which the HORMA domain binds a phosphorylated region of Atg13 and adopts a closed-loop inactive conformation, and, upon starvation, this binding site becomes dephosphorylated and the closed-loop opens allowing for Atg9 binding. Additionally, Rao *et al.* reported direct binding of Atg13 to high-curvature vesicles made from yeast polar lipid extracts *in vitro* (Rao et al., 2016), suggesting that an as-yet-unmapped domain of Atg13 could facilitate Atg13/Atg9-loaded vesicle association.

Although Atg13 seems to be a strong recruiter of Atg9 to the PAS, there are additional reported interactions between Atg9-loaded vesicles and other components of the AIC (Rao et al., 2016; Sekito et al., 2009). All these interactions are thought to be dynamic (He et al., 2008) and thus they may all cooperate in recruiting Atg9 to the PAS *in vivo*. Below, I discuss these additional interactions.

Atg1 phosphorylates Atg9 and may define the selectivity for high-curvature vesicles.

Upon activation, Atg1 phosphorylates at least 7 residues on the N- and C-terminal IDRs of Atg9 *in vivo* (Papinski et al., 2014), and *in vitro* and *in vivo* studies reported that the C-terminus of Atg9 binds Atg1 (Feng et al., 2016; Papinski et al., 2014), consistent with the existence of at least a transient interaction between the two proteins. In addition to binding Atg9, full-length Atg1 is specifically recruited to high curvature lipid vesicles in a co-floatation assay (Rao et al., 2016). This interaction may be mediated by the $Atg1^{EAT}$ motif, as this motif is competent to bind high curvature two vesicles *in vitro* (Ragusa et al., 2012). Of note, the assembled pentameric AIC showed the same high-curvature lipid vesicle binding specificity as the isolated Atg1-Atg13 heterodimer (Rao et al., 2016), suggesting that Atg1 and Atg13 might play an important role in the selective recruitment of high curvature Atg9-vesicles. Selecting highly curved lipid vesicles might be important for autophagosome formation, as these highly strained structures are inherently unstable and their fusion is energetically favorable (François-Martin et al., 2017). This is particularly relevant as no SNAREs have been found at the PAS, suggesting that vesicle fusion

may be spontaneous or is catalyzed by an unknown SNARE-independent mechanism (Reggiori et al., 2004b).

As discussed in Chapter 1, Atg13 is thought to regulate the rigidity Atg1's tMIT motif (Stjepanovic et al., 2014), raising the possibility Atg13-Atg1 binding could improve Atg1-Atg9 binding and allow for the subsequent Atg9 phosphorylation. Notably, Atg9 is thought to be absent from complete autophagosomes (Noda et al., 2000; Reggiori et al., 2004a), suggesting that it must be removed from the growing phagophore at some point before autophagosome closure. While the mechanism of this Atg9 retrieval and recycling is unknown, it is possible that Atg1 kinase activity is important in this recycling process, which is distinct from the Atg1-aided recruitment of Atg9-loaded vesicles to the PAS (Papinski et al., 2014; Sekito et al., 2009). Indeed, Atg1 kinase activity is dispensable for recruitment of Atg9 to the PAS (Sekito et al., 2009) and the interaction between Atg1 and Atg9 is dispensable for the activation of Atg1 kinase activity (Papinski et al., 2014) suggesting that phosphorylation occurs downstream of vesicle recruitment. Moreover, when kinase-defective alleles of Atg1 are expressed in an $Atg1^{-}$ background, Atg9 aberrantly accumulates at the PAS (Sekito et al., 2009). Together, these observations suggest that Atg1 phosphorylation of Atg9 may be linked to the downstream recycling of Atg9 back to the cytoplasm, but future work will be required to elucidate the exact mechanistic role of Atg9 phosphorylation.

Atg9-loaded vesicle binding to Atg17 requires the displacement of the Atg29/Atg31 dimer.

Ragusa *et al.* suggested a direct role of Atg17 in Atg9-loaded vesicle binding and tethering when they noticed a conspicuous similarity between the curvature of the concave faces of the crystallized Atg17 dimer observed radius of Atg9-loaded vesicles (Ragusa et al., 2012). The suggestion was supported by the reported *in vitro* binding between purified Atg17 and Atg9-loaded proteoliposomes (Rao et al., 2016). Atg17 did not, however, bind protein-free liposomes (Rao et al., 2016), suggesting either that Atg17 binds directly to Atg9, or that integration of Atg9 alters the proteoliposome conformation to facilitate Atg17 binding. Using Atg17 truncations, Rao *et al.* suggested that Atg17's binding site for Atg9-loaded vesicles is on concave face of the Atg17 dimer, which overlaps with Atg17's binding site for Atg29/Atg31 (Rao et al., 2016). Consistently, the Atg29/Atg31 complex was shown to reduce the Atg9-proteoliposome binding activity of Atg17, suggesting that Atg29/Atg31 and Atg9 compete for binding to Atg17 (Rao et al., 2016). How this

competition unfolds given the constituent's local concentration at the PAS is unknown, but *in vitro* and *in vivo* experiments suggest that Atg13 is needed to activate the Atg9-binding function of Atg17 (Rao et al., 2016). This observation, together with the reported competition between Atg13 and Atg31 for binding to Atg17 (Rao et al., 2016), led me to propose the following model for Atg9 binding to Atg17 (Figure 16): while the Atg29/Atg31 dimer is bound to Atg17 (Figure 16a), Atg9-loaded vesicles cannot bind to Atg17 due to a steric clash with the Atg29/Atg31 dimer (Figure 16b). Upon starvation, however, Atg13 displaces the Atg29/Atg31 dimer (containing Atg1-phosphorylated Atg29) from Atg17 as described in Chapter 3 (Figure 12a-j). Upon the Atg13-mediated displacement of the Atg29/Atg31 dimer (Figure 16c), the binding site for Atg9 on Atg17 becomes exposed, allowing Atg9 to bind to Atg17 (Figure 16d). I further propose that Atg13 does not compete with Atg9 for Atg17 binding, allowing Atg9 to simultaneously bind to Atg17 (Figure 16d inset).

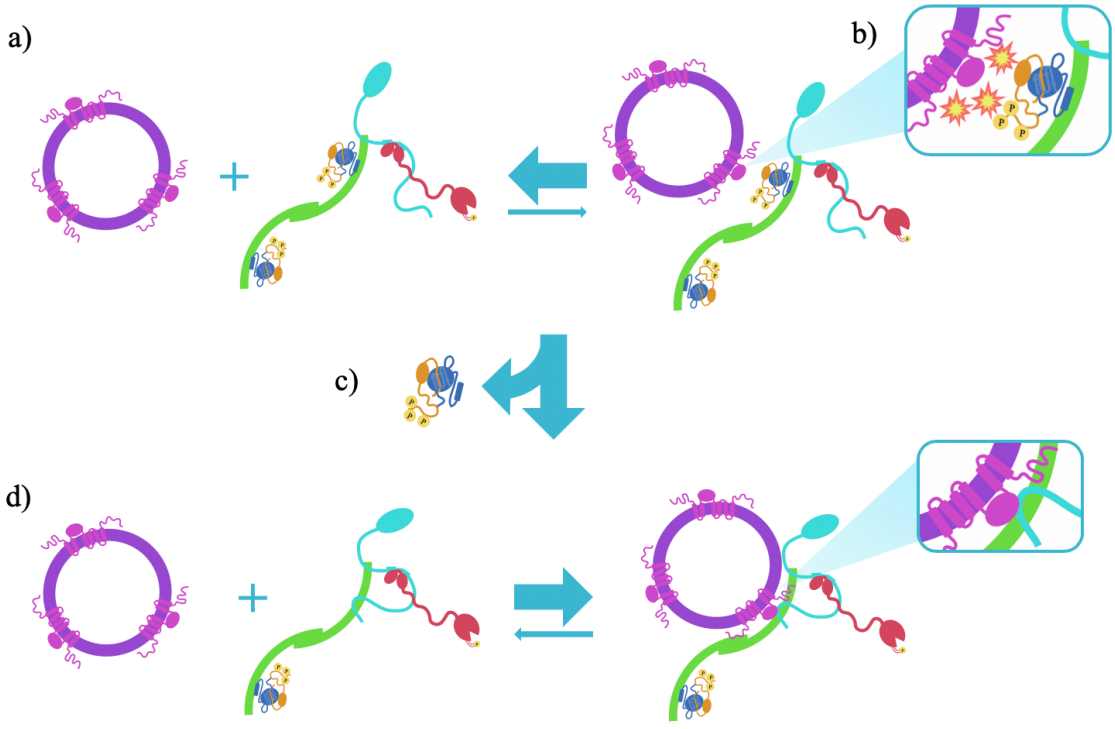

Figure 16: A model for Atg9 binding to Atg17. Binding of Atg9-loaded vesicles to Atg17 requires the Atg13-mediated displacement of the Atg29/Atg31 dimer. Of note, only the early Atg9 events are depicted. Downstream events will be depicted in subsequent figures.

A role for Atg9 self-association in vesicle recruitment to the PAS.

In addition to the members of the AIC discussed in the previous sections, Atg9 itself might assist with Atg9-loaded vesicle recruitment to the PAS via self-association between the Atg9 C-terminal IDRs (He et al., 2008). Under fed conditions, Atg9-loaded vesicles are thought to be mostly monomeric and to continually cycle between the cytoplasm and the PAS (Rao et al., 2016; Reggiori et al., 2004a; Sekito et al., 2009; Yamamoto et al., 2012). Upon starvation, however, Atg9-loaded vesicles are recruited to the PAS in an AIC-dependent manner (Sekito et al., 2009; Suzuki et al., 2015). This recruitment of Atg9-loaded vesicles to the PAS also depends on Atg9 self-association (He et al., 2008), suggesting that AIC-associated Atg9 might cooperatively recruit other Atg9-loaded vesicles to the PAS. I propose that the multiple interactions between Atg9-loaded vesicles and the different components of the AIC described above (including Atg9 itself) result in a highly cooperative PAS recruitment of subsequent Atg9-loaded vesicles, which could benefit the cell by allowing it to regulate this important step in autophagy in a switch-like manner.

Cooperative recruitment of Atg9 to the PAS may facilitate AIC-mediated tethering of Atg9-loaded vesicles.

The symmetric nature of the $(Atg17/Atg29/Atg31)_2$ dimer of trimers crystal structure suggests that each Atg17 monomer can bind one Atg9-loaded vesicles (Ragusa et al., 2012). Moreover, *in vitro* experiments showed that Atg17-Atg17 dimer can indeed bind 2 Atg9-loaded vesicles independently and function as a vesicle tether (Rao et al., 2016). Interestingly, although Atg9-containing proteoliposomes were polydisperse in solution by dynamic light scattering (DLS), suggesting that the Atg9-loaded vesicles are clustering, when these proteoliposomes were generated in the presence of Atg17, they became monodispersed with an R_H value corresponding to two tethered vesicles (Rao et al., 2016). This suggests that Atg17 can inhibit the higher-order clustering of Atg9-loaded vesicles, presumably by binding to Atg9 and competing with other Atg9-loaded vesicles for Atg9 binding. Although *in vitro* experiments showed that one Atg17 dimer can tether two Atg9-loaded vesicles, quantitative fluorescence counting of molecules at the PAS suggests that ~3 Atg9-loaded vesicles fuse to give rise to one autophagosome (Yamamoto et al., 2012), and that ~14 Atg17 dimers are present at the PAS (Köfinger et al., 2015). This means that at the PAS, there are roughly 5-fold more Atg17 dimers than there are Atg9-loaded vesicles. Thus, it seems unlikely that 2 Atg9 vesicles would end up on the same Atg17 dimer in the absence of

some form of positive cooperativity. I propose that, upon autophagy, a first Atg9-loaded vesicle binds to an Atg17 dimer at the PAS, and that this first binding event increases the probability of a second Atg9-loaded vesicle stably binding to the same Atg17 dimer by creating additional Atg9-Atg9 stabilizing interactions. As I will discuss at the end of this chapter, future work to determine whether an Atg17 dimer in fact binds two Atg9-loaded vesicles *in vivo* will be very important in unraveling the mechanism of AIC-mediated Atg9-loaded vesicle fusion.

Open questions on the interaction between Atg9 and the AIC.

As discussed above, Atg9 oligomerization is thought to be mediated by its C-terminal IDR, as truncations in this region disrupt Atg9 self-association (He et al., 2008). An important open question is whether starvation also increases Atg9 oligomerization in an intra-vesicular manner and, if so, how it is regulated. Of note, the C-terminal IDR of Atg9 contains several Atg1 phosphorylation sites (Papinski et al., 2014), suggesting that Atg1 may play a regulatory role in Atg9 self-association. Although the mechanistic role of Atg1-mediated Atg9 phosphorylation is yet to be elucidated, below I propose a mechanism for Atg9 fusion in which Atg1-mediated phosphorylation of the C-terminal IDR of Atg9 facilitates intra-vesicular Atg9 oligomerization (Figure 17), facilitating the concentration of Atg9 molecules on the one side of the vesicle and the generation of Atg9-free regions on the vesicle that allow for fusion.

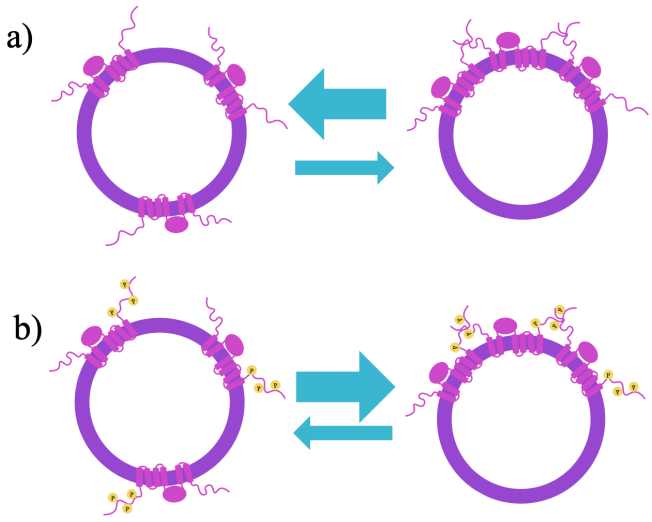

Figure 17: A proposed role for Atg1-mediated Atg9 phosphorylation. **a)** In the absence of phosphorylation, Atg9 molecules freely diffuse in the lipid vesicle. **b)** Atg1 phosphorylation of the C-terminal IDR of Atg9 induces intra-vesicular Atg9 oligomerization. Of note Atg9 oligomerization exposes Atg9-free lipid regions on the vesicle that could then touch another Atg9-free region in a different vesicle and fuse.

A model for Atg9-loaded vesicle PAS recruitment and fusion.

Based on the observations described above, I propose the following model for Atg9 PAS recruitment and fusion: Under fed conditions, the ~27 Atg9 molecules in the Atg9-loaded vesicles

are homogeneously distributed on the lipid membrane, effectively blocking vesicle fusion through lipid-lipid contacts whenever these vesicles encounter one another (Figure 17a). Upon starvation, however, the AIC forms as described in Chapter 3 (Figure 12), activating the AIC components for Atg9-loaded vesicle recruitment as follows: i) the Atg1 kinase becomes activated, as described in Chapter 3, and it phosphorylates Atg29 (Figure 12g-i); ii) as described in Chapter 3, upon Atg29 phosphorylation, Atg13 displaces the Atg29/Atg31 dimer from Atg17, resulting in the formation of Atg9-binding capable Atg17 dimers (Figure 12j and Figure 16); iii) Atg13 dephosphorylation causes a conformational change in Atg13 that exposes the HORMA domain, allowing it to bind Atg9-loaded vesicles; iv) upon Atg13 dephosphorylation, Atg13 binds to and stabilizes the EAT motif on Atg1, which can then bind exposed high curvature membranes of the Atg9-loaded vesicles. Importantly, this selective binding to high curvature membranes could provide quality control of this process by ensuring that only high-curvature Atg9-loaded membrane vesicles, and not other cellular vesicles such as endosomes (Reggiori et al., 2004b), are recruited to the PAS and eventually integrated into autophagosomes.

Once Atg1, Atg13 and Atg17 have been activated for Atg9-loaded vesicle binding, I propose that the three proteins cooperate to recruit the first Atg9-loaded vesicles to the PAS (Figure 18a); Once Atg9-vesicles are at the PAS, the active Atg1 kinase phosphorylates Atg9's C-terminal IDR (Figure 18b), inducing intra-vesicular Atg9 oligomerization (Figure 18c). Simultaneous binding of Atg1 and Atg13 to the lipid part of the vesicle, direct binding of Atg17 to Atg9, and the Atg13-mediated crosslinking of Atg17 dimers further helps to concentrate Atg9 on one side of the lipid vesicle, forming Atg9-free and Atg9-rich patches on the Atg9-loaded vesicles (Figure 18d). Eventually, through Atg9 self-interactions, the first Atg9-loaded vesicle helps to recruit a second Atg9-loaded vesicle to the same Atg17 dimer (Figure 18e). Finally, I propose that, in the absence of the Atg29/Atg31 dimer, Atg17 becomes more flexible, allowing for a conformational change that brings the two Atg9-loaded vesicles in close proximity (Figure 18f), causing their fusion (Figure 18g). Importantly, I propose that the formation of Atg9-free and Atg9-rich patches on the Atg9-loaded membranes helps to 1) create Atg9-free zones that more easily fuse with each other (Figure 18f) and 2) help to concentrate Atg9 at one side of the forming phagophore (Figure 18g). I further propose that Atg9 prefers high curvature membranes and by passively migrating and preferentially residing in high-curvature membrane, it can stay at the most highly-curved region

of the nascent phagophore once the vesicles fuse. Further, I propose that this high curvature regions help to keep the growing phagophore bound to Atg17 dimers (Figure 18g), facilitating iteration of the process and the subsequent fusion of a third Atg9-loaded vesicle (Figure 18h).

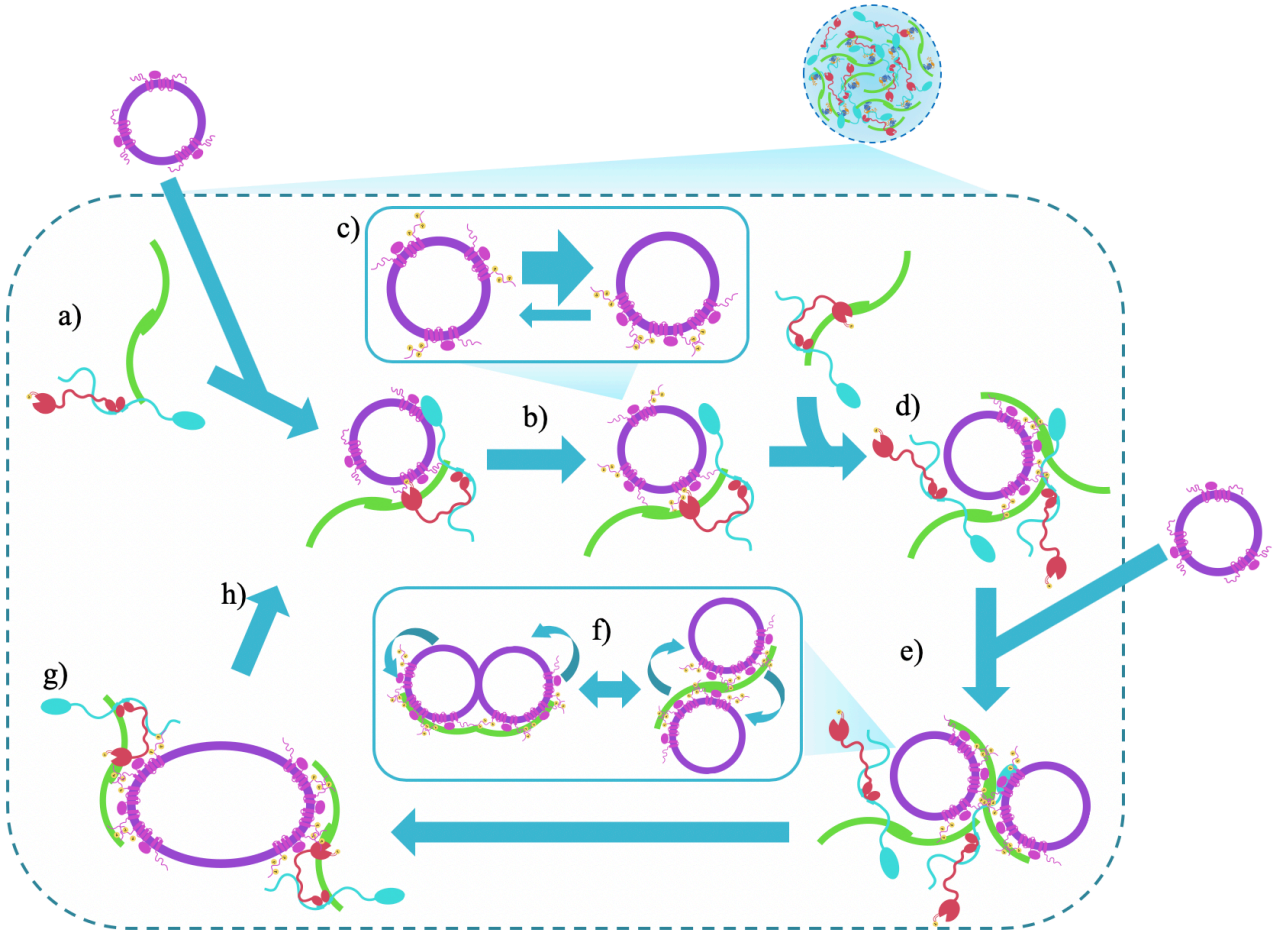

Figure 18: A model for AIC-mediated Atg9-loaded vesicle fusion. **a)** The pentameric and activated AIC cooperatively recruits Atg9-vesicles; **b)** Once the Atg9-vesicle is recruited to the PAS, Atg1 phosphorylates Atg9 at its C-terminal IDR. **c)** Atg9-phosphorylation induces intra-vesicular Atg9 self-assembly. **d)** The AIC forms supramolecular complexes via Atg13-mediated crosslinking, which facilitates the exposure of Atg9-free lipid regions on the Atg9-vesicle. **e)** Atg9 self-association helps to recruit a second Atg9-vesicle to the same Atg17 dimer, which also exposes Atg9-free regions. **f)** Once both Atg9-vesicles are bound to the same Atg17 dimer, their now exposed lipid regions can meet through an Atg17 conformation change, facilitating their fusion. **g)** Of note, Atg9 stays at the most highly curved region of the growing phagophore. **h)** The cycle is repeated to facilitate the fusion of a third Atg9-vesicle to the growing phagophore.

Chapter 5: A single-molecule approach to study the AIC

As I have discussed in Chapters 1-4, AIC formation is a highly regulated decision-making step in starvation-induced autophagy (Chang and Neufeld, 2009; Kamada et al., 2000; Stephan et al., 2009) and thus a key step for the development of therapeutic agents that modulate autophagy. Nevertheless, our detailed mechanistic understanding of AIC assembly and of its putative role in Atg9-vesicle fusion are currently limited. Given the number of components of the AIC and the different oligomeric states that these components can have (He et al., 2008; Köfinger et al., 2015; Ragusa et al., 2012; Yamamoto et al., 2016), it is likely that AIC formation is not a linear pathway, but rather, a network of interconnected parallel binding reactions. Similar, highly parallel assembly pathways have been observed in other large macromolecular complexes such as the bacterial ribosome (Davis et al., 2016). If true, the cell could use these parallel pathways to more quickly assemble the AIC upon starvation and more quickly disassemble it once nutrients are replenished. As described in the preceding chapters, there is significant evidence for such parallelism and complex heterogeneity, which has made it challenging to study the AIC using bulk biochemical approaches as these techniques often obscure crucial mechanistic features of the lower abundance assembly pathways. Additionally, our poor understanding of this heterogeneity may also hinder future work to develop therapeutic agents, as the inhibition of some seemingly important protein-protein interactions by a therapeutic drug could be bypassed via alternative parallel pathways.

The need to characterize all the possible AIC assembly mechanisms motivated our group to develop a single-molecule fluorescence microscopy approach to study the AIC. As discussed below, this new approach will allow us to identify multiple AIC assembly orders, to quantify the number of molecules of each component in the AIC, and to determine the kinetics, cooperativity, and competition of AIC protein association. Further, this single-molecule approach will allow us to study the roles of disease, phospho-mimetic and phospho-null mutations on AIC assembly and function. Thus, this single-molecule approach has great potential to help us answer some of the important outstanding questions that I discussed in the previous chapters. Below, I describe some of the progress that I have made towards developing this new approach to study the AIC.

A single-molecule fluorescence microscopy assay to study Atg17 dimerization.

In preliminary experiments aimed at developing a single-molecule assay, I focused on Atg17, given its putative role as the master PAS organizer discussed in Chapter 2 (Suzuki et al., 2007). Specifically, I wanted to start by measuring the unknown kinetic parameters of Atg17 dimerization. In the following sections, I describe development of this assay in detail, but first, I provide a brief overview (Figure 19). First, a SNAP-protein tag (Keppler et al., 2003) was fused (Joey Davis, personal communication) to the N-terminus of Atg17 that allowed me to covalently label Atg17 with biotin or with fluorescent dyes (Figure 19a). Then, I used streptavidin-coated microscope slides to attach the biotinylated SNAP-Atg17 to the slide surface (Figure 19b). Finally, to obtain single-molecule resolution, I employed total internal reflection fluorescence (TIRF) microscopy, a technique that primarily illuminates fluorescent molecules within ~100nm of the microscope slide, greatly enhancing the signal-to-noise ratio and allowing for imaging of single-molecules when samples are applied in the pM–nM concentration range (Kudalkar et al., 2016a). Thus, after adding dye-labeled Atg17 to pre-attached biotinylated SNAP-Atg17, I expect to observe a fluorescent spot every time that a dye-labeled SNAP-Atg17 molecule approaches, binds, and resides near the microscope slide longer than the acquisition time. Such events include dimerization between a dye-labeled SNAP-Atg17 and a biotinylated SNAP-Atg17 as well as non-specific association between dye-labeled SNAP-Atg17 and either the glass slide or the passivating

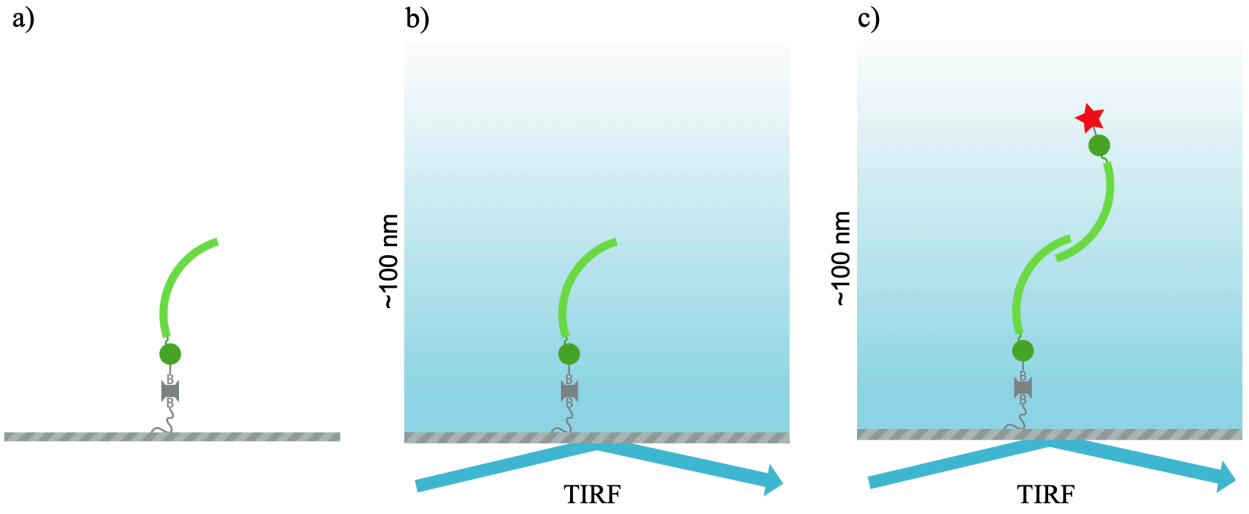

Figure 19: A single-molecule assay to study Atg17 dimerization. **a)** A biotinylated SNAP-Atg17 molecule is fixed to a streptavidin-coated slide. **b)** TIRF microscopy illuminates ~100 nm into the sample with exponentially decaying intensity, providing single-molecule resolution. **c)** Dye-labeled SNAP-Atg17 is flowed onto the pre-attached Atg17 monomer, causing a fluorescent spot in the image every time a dye-labeled SNAP-Atg17 molecule dimerizes with a biotinylated SNAP-Atg17 molecule.

PEG molecules attached to the glass (Figure 19c). Further, by analyzing the lengths of time that Atg17 spends in the on and off states, I can calculate kinetic dissociation and association constants, respectively (Kinz-Thompson et al., 2016), and use these constants to calculate thermodynamic K_D values. Below, I will describe in detail every step of the assay.

Generating protein constructs for initial proof-of-concept experiments.

The first step in the development of this assay was to label Atg17 with a fluorescent tag. This was achieved by genetically fusing a 20 kDa protein tag, called SNAP tag, to the N-terminus of Atg17, subsequently referred to as SNAP-Atg17 (Figure 20a). This tag is a mutated version of a bacterial DNA repair protein O^6-alkylguanine-DNA alkyltransferase that selectively reacts with benzylguanine (BG) derivatives, resulting in irreversible covalent labeling of the protein (Keppler et al., 2003). In this assay, I used the SNAP tag to label our SNAP-Atg17 construct with SNAP-Biotin®, and two different fluorescent dyes, SNAP-Surface® 488 and SNAP-Surface® 649 (~Cy5).

Previously, Ragusa *et al.* showed that truncating the C-terminal dimerization helix of a thermophilic Atg17 homolog rendered the protein monomeric in solution, and they also showed that the homologous truncation in the highly conserved C-terminal helix caused defects in autophagic activity in *S. cerevisiae* (Ragusa et al., 2012). Thus, as a negative control for Atg17 dimerization, I generated a C-terminally truncated version of *S. cerevisiae* Atg17 lacking the C-terminal 59 amino acids of the dimerization helix (referred to as SNAP-Atg17ΔC1, Figure 20b) with the expectation that this construct would be monomeric. Notably, the oligomeric state for the S. cerevisiae truncated protein has not been reported. To determine the oligomeric state of this construct, I expressed and purified each variant from *E. coli* and ran each sample on an analytical gel-filtration column at

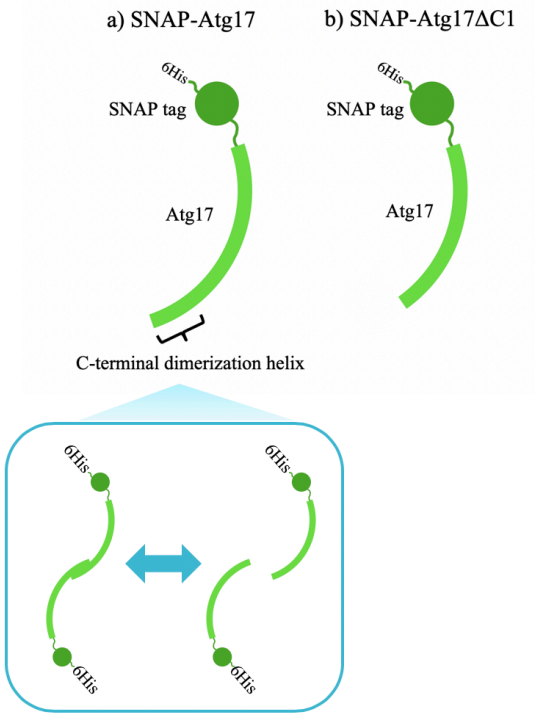

Figure 20: Initial constructs used in assay validation. **a)** Dimerization-capable SNAP-Atg17. **b)** Monomeric SNAP-Atg17.

equal concentrations. As shown in Figure 21, the C-terminal truncation caused a delay in the protein's elution, suggesting that the truncation does in fact disrupt *S. cerevisiae* Atg17 dimerization. Of note, both proteins appear to run larger than a monomer or dimer, respectively, consistent with a highly extended conformation (Ragusa et al., 2012).

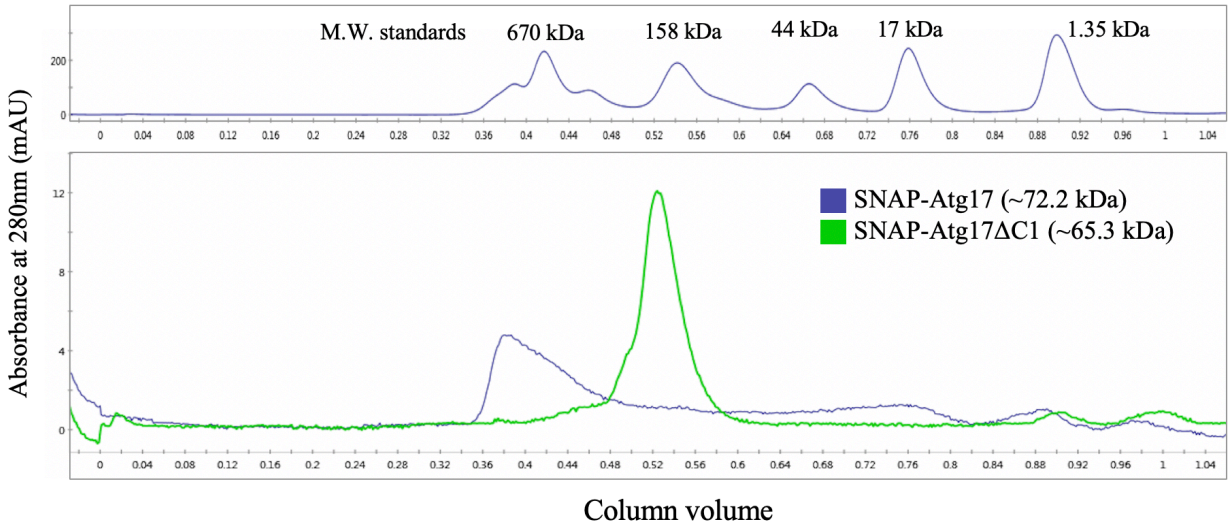

Figure 21: SNAP-Atg17ΔC1 is a monomer in solution. Gel filtration profiles of the constructs described in Figure 20. The shift in the elution volume of the C-terminally truncated SNAP-Atg17ΔC1 is consistent with the construct being a monomer in solution. Top panel shows molecular weight standards.

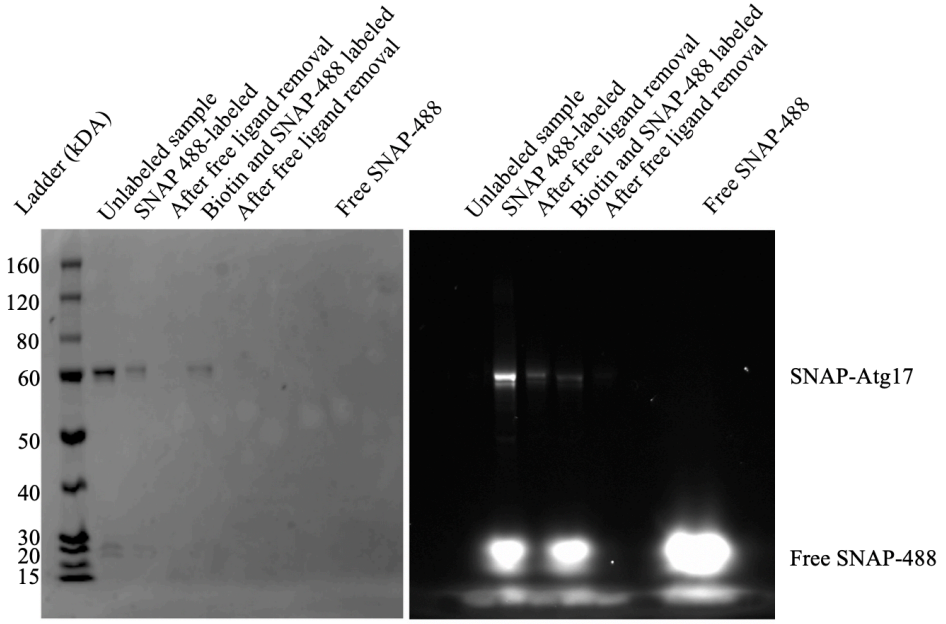

Figure 22: Labeling of SNAP-Atg17 with SNAP ligands. **a)** Coomassie brilliant blue stain of gel monitoring the different stages of the labeling reaction and free ligand separation. **b)** In-gel fluorescence of gel shown in **a)** with excitation targeting the SNAP-488 dye.

Protein labeling and separation of free ligands.

After optimizing the purification conditions for SNAP-Atg17, we proceeded to label the protein with SNAP-Biotin and SNAP-488, and found that the recombinant protein can be labeled, suggesting that, at a minimum, the SNAP domain is properly folded (Figure 22). After labeling, I separated the free SNAP-ligands from the labeled protein using a Zeba™ spin desalting column. Although quantification of the in-gel fluorescence bands with ImageJ™ showed an that only ~20% of the labeled protein could be recovered, the column quantitatively removed free dye (Figure 22). As I will discuss above, our single-molecule experiments required very low protein concentrations and this protein loss was not an issue.

Atg17 may not be a constitutive dimer in solution.

Given the possibility that Atg17 could be a constitutive dimer (Chew et al., 2013; Köfinger et al., 2015; Rao et al., 2016), in initial experiments, I labeled SNAP-Atg17 with SNAP-Biotin and SNAP-488 in the same reaction to obtain a population of dual-labeled Atg17 dimers such as those shown on Figure 19c. I then acquired smTIRF images, and, excitingly, observed ~100-200 single-molecule spots. This observation is consistent with Atg17 dimers bearing a SNAP-488 in one subunit and a SNAP-Biotin in the other. Collecting a time-series movie of the slides revealed that the fluorescent spots that appeared and disappeared over time, suggesting that Atg17-SNAP488 could be dissociating and re-associating with a tethered Atg17-SNAP-Biotin, consistent with a dynamic Atg17 dimer. For this reason, in future experiments, I separately labeled SNAP-Atg17 with SNAP-Biotin and with SNAP-dye, and then mixed them in a 1:1 ratio with expectation that they would exchange in solution.

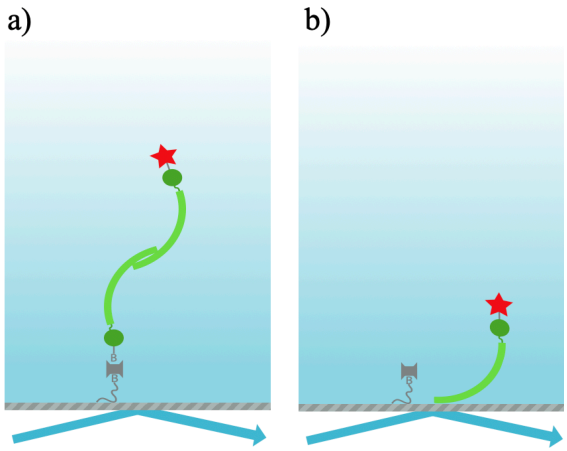

Figure 23: Two possible interpretation of appearance and disappearance of fluorescent spots in single-molecule experiments. **a)** Specific dimerization between a SNAP-Atg17 monomer labeled with a fluorescent dye and a biotinylated SNAP-Atg17 monomer attached to microscope slide. **b)** Non-specific binding of SNAP-Atg17 labeled with a florescent dye to the microscope slide.

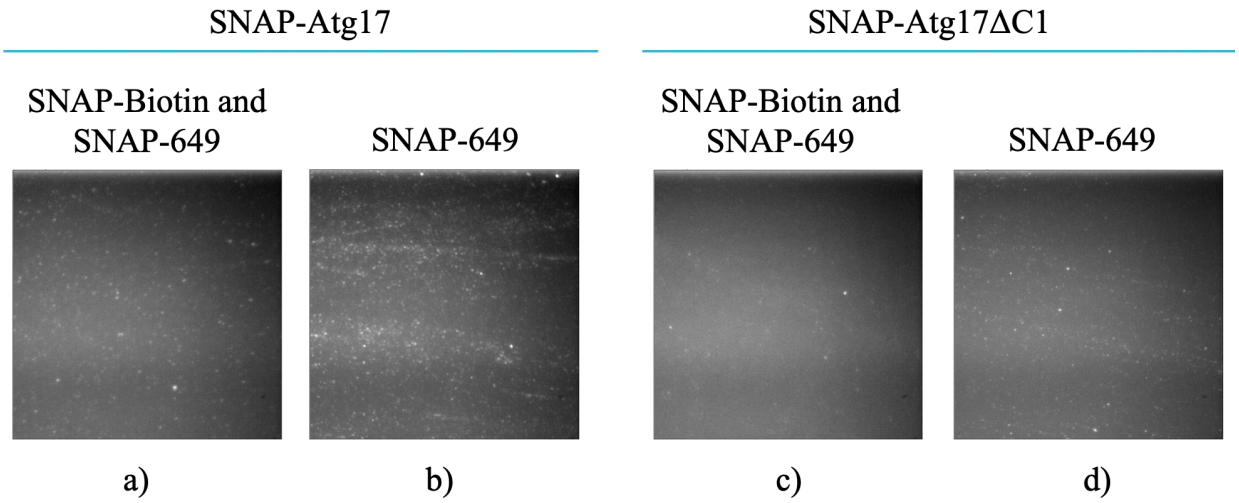

Figure 24: SNAP-Atg17 and SNAP-Atg17ΔC1 bind to the microscope slide non-specifically. Images are the integration of first 50 frames of videos acquired on TIRF microscope. Total protein concentrations are the same across all samples. **a)** 1:1 mixture of biotinylated SNAP-Atg17 and SNAP-649-labeled SNAP-ATG17; **b)** SNAP-649-labeled SNAP-Atg17; **c)** 1:1 mixture of biotinylated SNAP-Atg17ΔC1 and SNAP-649-labeled SNAP-ATG17 ΔC1; **d)** SNAP-649-labeled SNAP-Atg17ΔC1.

In these experiments, I interpret the appearance and disappearance of a fluorescent spot as Atg17 dimerization and dissociation, respectively (Figure 23a). Alternatively, it is possible that Atg17 is non-specifically binding to the microscope slide (Figure 23b). To test this alternative interpretation, I performed two important control experiments. First, I imaged a sample to which we did not add biotinylated SNAP-Atg17 (Figure 24b) and second, I repeated the experiment with SNAP-Atg17ΔC1, which I previously showed is be monomeric (Figure 24c-d). Although we expected to see only a few spots, if any, in these control experiments, we observed many spots, suggesting that SNAP-Atg17 and SNAP-Atg17ΔC1 non-specifically bind to the microscope slide. Interestingly, I actually observed more spots in the absence of biotinylated SNAP-Atg17, but I was unable to determine the origin of this anomaly. In future experiments, I will screen various buffers, slide treatments, and dye-labels for conditions that limit this non-specific SNAP-Atg17 binding. Of note, in initial buffer tests, I repeated the experiments adding either 10% glycerol or 3% bovine serum albumin (BSA), but I obtained similar results.

Data analysis.

Although I am working to find conditions that reduce non-specific binding, I simultaneously worked to develop an in-house Python script to analyze the smTIRF videos that I acquired. My data analysis using this Python script is summarized in Figure 25. Briefly, I take the

TIFF videos acquired from the microscope, containing 200-2000 frames (Figure 25a). To increase the signal-to-noise ratio and more easily find spots, I integrate ~30-60 consecutive frames and find spots using a difference of gaussian model (Figure 25b). To maximize the number of spots found, I iterate this process over the entire length of the video, obtaining a total of 100-200 spots (Figure 25c). Since the background fluorescence was not constant everywhere in the frame or between frames, my script subtracts the local background from each spot in each frame. To achieve this, I draw a donut-shaped area around each spot (Figure 25d), calculate the average fluorescence intensity in this donut and subtract it from the spot intensity in each frame, thus normalizing for spatial and temporal differences in background intensity. Then, by plotting fluorescence intensity vs. time, I obtain single-molecule traces like the one shown in Figure 25e. Of note, these traces start at the background, go up in intensity when a fluorescent molecule binds, and go back down to the background when the fluorescent molecule dissociates. In order to get more rigorous quantitation of the lengths of time that each fluorescent molecule spends in the bound state (further referred to as *dwell times*), I need to assign a state to each frame in the movie. In order to do this in a more unbiased way, I use a two-state hidden Markov model (HMM) to fit the single-molecule traces. HMMs are a common statistical way to assign a state (bound or unbound) to each frame and thus discretize our traces (Kinz-Thompson et al., 2016) (Figure 25f). Finally, I pooled all the calculated bound dwell times and calculated a dissociation constant by fitting their cumulative probability density function to a single exponential curve (Figure 25g) (Kinz-Thompson et al., 2016). This script, which is fully functional and will be used to analyze future data, is available at https://github.com/jhdavislab.

Concluding remarks on single-molecule assay development and path forward.

As discussed above, the most important next steps to optimize this assay are to find conditions that reduce or eliminate SNAP-Atg17 non-specific binding to the microscope slide. These experiments will include testing different detergent and salt conditions in the TIRF buffers (Pan et al., 2015), making microscope slides with different surface passivation treatments (for instance, testing different lengths of poly-ethylene glycol (PEG) and increasing the number of PEGylation steps), assaying the effect of different dyes, testing different relative ratios of biotinylated and dye-labeled protein concentrations, and adding additional surface blocking steps, such as the addition of bovine serum albumin (BSA) at different stages of sample preparation

(Kudalkar et al., 2016b). In addition to screening buffers, I will try to find ways to biotinylate and dye-label one Atg17 monomer with one color, and the other monomer with a different color. If possible, such an approach would allow me to selectively analyze binding events that show colocalization of both colors (representing specific Atg17 dimerization events), while discarding binding events showing one color (representing non-specific Atg17 binding to the microscope slide).

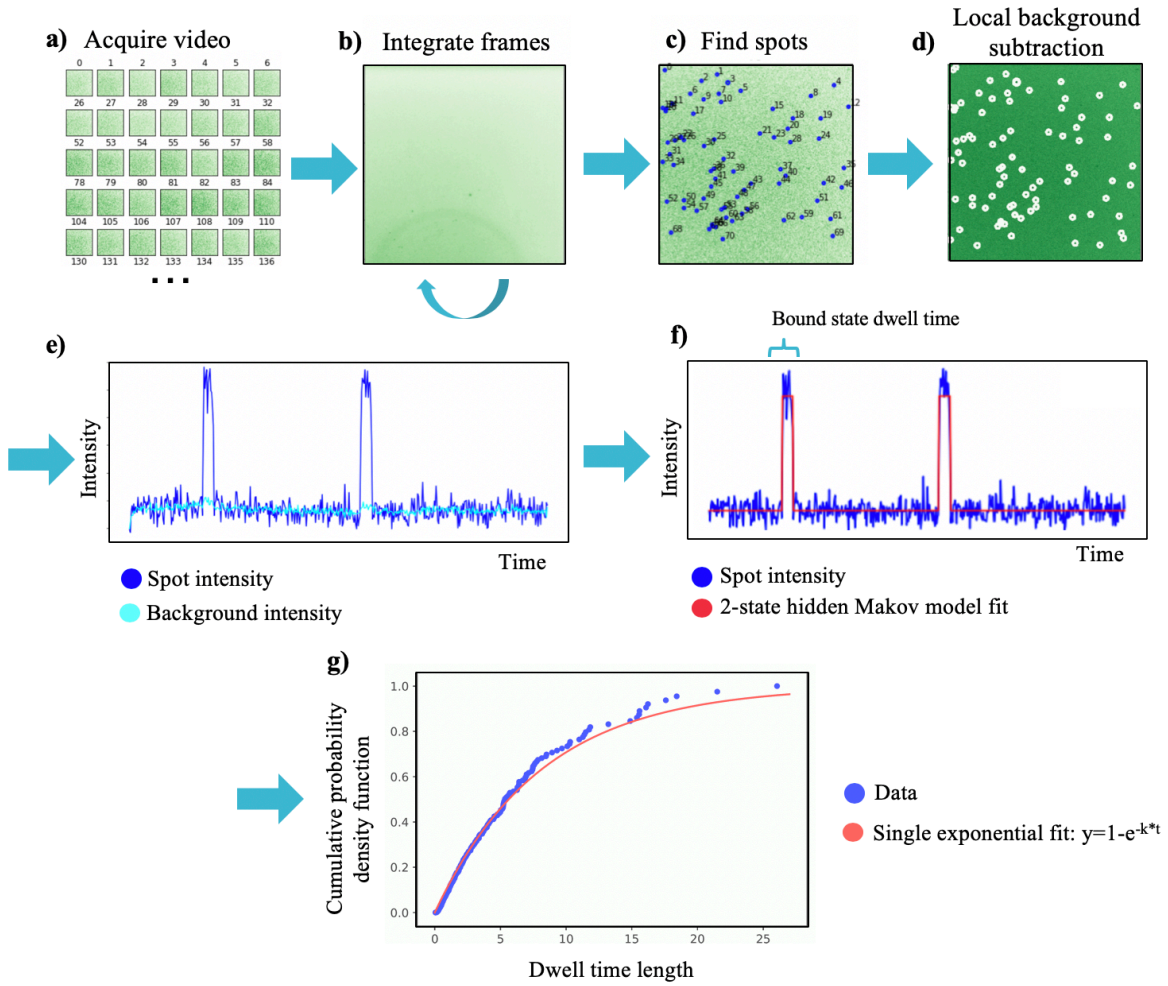

Figure 25: Developing a Python script for smTIRF data analysis. **(a)** Our script takes acquired TIFF files and **(b)** integrates 30-60 frames at the time to find spots. **(c)** Iterating this process throughout the length of the video gives us 100-200 spots. **(d)** Local background subtraction in each frame yields single-molecule traces **(e)** that are then fit to a two-state hidden Markov model **(f)** for more rigorous dwell time measurement. **(g)** Analysis of dwell times allows us to calculate dissociation constants.

Although this single-molecule assay needs further optimization, my preliminary results are promising. Once the assay is fully optimized, it will allow us to obtain kinetic and thermodynamic parameters on Atg17 dimerization. Further, by including other AIC components labeled with different colors and monitoring their colocalization with Atg17 over time, we will be able to elucidate the allowed binding orders in AIC assembly and calculate kinetic and thermodynamic constants (Kinz-Thompson et al., 2016) on AIC assembly. Of note, by adding the AIC components in different orders, we will be able to study how they interact with one another and calculate any cooperativity or competition in AIC assembly, and the single-molecule resolution of our assay will allow us to observe and classify lower-abundance behaviors on AIC assembly that are often overlooked in bulk approaches. Finally, using calibrated fluorescence, we will be able count the number of each component of the AIC. Thus, our new approach to study the AIC has the potential to provide us with unprecedented mechanistic insights on AIC is assemble and function, and may allow us to answer many of the open questions that I have discussed throughout this work.

Experimental methods

Construct generation.

SNAP-Atg17 and SNAP-Atg17-*ΔC* was cloned into a pET28a vector, with the addition of an N-terminal 6xHis tag for purification and a thrombin cleavage site between the 6xHis tag and the SNAP-tag, transformed into DH5α *E. coli* for plasmid propagation, purified and sequenced. SNAP-Atg17-*ΔC* was generated by round-the-horn mutagenesis of pET28a 6xHis-Thrombin-SNAP-Atg17, the reaction was digested with Dpn1, phosphorylated and ligated using a KLD Enzyme Mix (NEB Cat. # M0554S), transformed into *DH5α E. coli* for plasmid propagation, purified and sequenced.

Protein expression and purification.

Purified plasmids were transformed into TSS-competent Tuner™ (DE3) *E. coli.* Cells were grown in 2xYT media supplemented with 0.2% glucose at 37°C to OD600=0.8-1 and protein production was induced with 1mM IPTG for 16-20h at 16°C. Cell pellets were snap-frozen in liquid nitrogen, cryogenically ground using a Retsch mixer-mill, resuspended in lysis buffer (using 3 mL of buffer/1 g of cell weight) and sonicated. Protein was purified in batch with Ni Sepharose™ resin (0.5 mL resin/1L of cell culture) pre-equilibrated in lysis buffer, washed with 100 column volumes of wash buffer and eluted with 10 column volumes of elution buffer. Elution fractions were assayed for protein using Bradford dye, and positive fractions were then injected on an S200 10/300 gel filtration column pre-equilibrated in gel filtration buffer.

Analytical gel filtration.

Protein sample concentrations were normalized to 2.2 µM total protein concentration in gel filtration buffer and run on an S200 10/60 column. Molecular weight standards were purchased from Biorad (catalog # 1511901).

Protein labeling and separation of free dye.

Proteins were labeled with SNAP-Surface® Biotin, SNAP-Surface® 549 and SNAP-Surface® 488 in 50µl reactions in gel filtration buffer as follows. Labeling reagent (6.25 µM), protein (2.75 µM, total protein concentration), and dithiothreitol (1 M) were mixed and incubated room temperature for 120 minutes. After labeling, the whole reaction was applied to a Zeba™ Spin Desalting Columns, 7K MWCO, 0.5 mL (ThermoFisher, catalog # 89882) to separate free from bound SNAP-ligand following the manufacturer's protocol. The entire 50µl reaction volume was flowed through the column, with an added 15 µl chase of gel filtration buffer (see manufacturer's protocol).

TIRF microscopy.

Samples were taken directly from Zeba™ Spin Desalting Columns, diluted 1:100 in TIRF buffer and combined as specified in Figure 23. Samples were then loaded onto streptavidin-coated microscope slides (Microsurfaces Inc. Cat. # Strept_01) and imaged on a Nikon Eclipse Ti inverted

microscope using a 60X TIRF objective, 100 nm penetration depth and 14.49 ms/frame acquisition time. Integrated images were generated on ImageJ™.

Buffers.

Lysis: 50 mM Tris, 500 mM NaCl, 10% glycerol, 20 mM imidazole, 5 mM βME, 1 mM PMSF [pH 8.0].
Wash: 50 mM Tris, 500 mM NaCl, 10% glycerol, 40 mM imidazole, 5 mM βME [pH 8.0].
Elution: 50 mM Tris, 500 mM NaCl, 10% glycerol, 250 mM imidazole, 5 mM βME [pH 8.0].
Gel filtration: 50 mM Tris, 150 mM NaCl, 10 mM KCl, 1 mM DTT [pH 7.4].
TIRF: 50 mM Tris, pH 8, 125 mM NaCl, 10% glycerol. 1 mM DTT, [pH 8.0].

References

Belle, A., Weissman, J.S., Ghaemmaghami, S., Bower, K., Huh, W.-K., Dephoure, N., O'Shea, E.K., and Howson, R.W. (2003). Global analysis of protein expression in yeast. Nature *425*, 737–741.

Bento, C.F., Renna, M., Ghislat, G., Puri, C., Ashkenazi, A., Vicinanza, M., Menzies, F.M., and Rubinsztein, D.C. (2016). Mammalian Autophagy: How Does It Work? Annu. Rev. Biochem. *85*, 685–713.

Boeynaems, S., Alberti, S., Fawzi, N.L., Mittag, T., Polymenidou, M., Rousseau, F., Schymkowitz, J., Shorter, J., Wolozin, B., Van Den Bosch, L., et al. (2018). Protein Phase Separation: A New Phase in Cell Biology. Trends Cell Biol. *28*, 420–435.

Budovskaya, Y. V., Stephan, J.S., Deminoff, S.J., and Herman, P.K. (2005). An evolutionary proteomics approach identifies substrates of the cAMP-dependent protein kinase. Proc. Natl. Acad. Sci. *102*, 13933–13938.

Chang, Y.-Y., and Neufeld, T.P. (2009). An Atg1/Atg13 Complex with Multiple Roles in TOR-mediated Autophagy Regulation. Mol. Biol. Cell *20*, 2004–2014.

Cheong, H., Nair, U., Geng, J., and Klionsky, D.J. (2008). The Atg1 Kinase Complex Is Involved in the Regulation of Protein Recruitment to Initiate Sequestering Vesicle Formation for Nonspecific Autophagy in Saccharomyces cerevisiae Heesun. Mol. Biol. Cell *19*, 668–681.

Chew, L.H., Setiaputra, D., Klionsky, D.J., and Yip, C.K. (2013). Structural characterization of the Saccharomyces cerevisiae autophagy regulatory complex Atg17-Atg31-Atg29. Autophagy *9*, 1467–1474.

Chew LH, Lu S, Liu X, Li FK, Yu AY, Klionsky DJ, Dong MQ, and Yip CK (2015). Molecular interactions of the Saccharomyces cerevisiae Atg1 complex provide insights into assembly and regulatory mechanisms. Autophagy *11*, 891–905.

Davis, J.H., Tan, Y.Z., Carragher, B., Potter, C.S., Lyumkis, D., and Williamson, J.R. (2016). Modular Assembly of the Bacterial Large Ribosomal Subunit. Cell *167*, 1610-1622.e15.

Fahs, S., Lujan, P., and Köhn, M. (2016). Approaches to study phosphatases. ACS Chem. Biol. *11*, 2944–2961.

Feng, W., Wu, T., Dan, X., Chen, Y., Li, L., Chen, S., Miao, D., Deng, H., Gong, X., and Yu, L. (2015). Phosphorylation of Atg31 is required for autophagy. Protein Cell *6*, 288–296.

Feng, Y., Backues, S.K., Baba, M., Heo, J.M., Harper, J.W., and Klionsky, D.J. (2016). Phosphorylation of Atg9 regulates movement to the phagophore assembly site and the rate of autophagosome formation. Autophagy *12*, 648–658.

Flint, A.J., Tiganis, T., Barford, D., and Tonks, N.K. (1997). Development of '"substrate-trapping"' mutants to identify physiological substrates of protein tyrosine phosphatases. Proc. Natl. Acad. Sci. *94*, 1680–1685.

François-Martin, C., Rothman, J.E., and Pincet, F. (2017). Low energy cost for optimal speed and control of membrane fusion. Proc. Natl. Acad. Sci. *114*, 1238–1241.

Fujioka, Y., Suzuki, S.W., Yamamoto, H., Kondo-Kakuta, C., Kimura, Y., Hirano, H., Akada, R., Inagaki, F., Ohsumi, Y., and Noda, N.N. (2014). Structural basis of starvation-induced assembly of the autophagy initiation complex. Nat. Struct. Mol. Biol. *21*, 513–521.

Galluzzi, L., Pietrocola, F., Bravo-San Pedro, J.M., Amaravadi, R.K., Baehrecke, E.H., Cecconi, F., Codogno, P., Debnath, J., Gewirtz, D.A., Karantza, V., et al. (2015). Autophagy in malignant transformation and cancer progression. EMBO J. *34*, 856–880.

Gomes, L.C., and Dikic, I. (2014). Autophagy in antimicrobial immunity. Mol. Cell *54*, 224–233.

He, C.K.J.D. (2010). Regulation Mechanisms and Signaling Pathways of Autophagy. Annu. Rev. Genet. *43*, 67–93.

He, C., Baba, M., Cao, Y., and Klionsky, D.J. (2008). Self-Interaction Is Critical for Atg9 Transport and Function at the Phagophore Assembly Site during Autophagy. Mol. Biol. Cell *19*, 5506–5516.

Hurley, J.H., and Young, L.N. (2017). Mechanisms of Autophagy. Annu. Rev. Biochem. *86*, 225--244.

Jao, C.C., Ragusa, M.J., Stanley, R.E., and Hurley, J.H. (2013). A HORMA domain in Atg13 mediates PI 3-kinase recruitment in autophagy. Proc. Natl. Acad. Sci. *110*, 5486–5491.

Kabeya, Y., Kamada, Y., Baba, M., Takikawa, H., Sasaki, M., and Ohsumi, Y. (2005). Atg17 Functions in Cooperation with Atg1 and Atg13 in Yeast Autophagy. Mol. Biol. Cell *16*, 2544–2553.

Kabeya, Y., Kawamata, T., Suzuki, K., and Ohsumi, Y. (2007). Cis1/Atg31 is required for autophagosome formation in Saccharomyces cerevisiae. Biochem. Biophys. Res. Commun. *356*, 405–410.

Kabeya, Y., Noda, N.N., Fujioka, Y., Suzuki, K., Inagaki, F., and Ohsumi, Y. (2009). Characterization of the Atg17-Atg29-Atg31 complex specifically required for starvation-induced autophagy in Saccharomyces cerevisiae. Biochem. Biophys. Res. Commun. *389*, 612–615.

Kamada, Y., Funakoshi, T., Shintani, T., Nagano, K., Ohsumi, M., and Ohsumi, Y. (2000). Tor-mediated induction of autophagy via an Apg1 protein kinase complex. J. Cell Biol. *150*, 1507–1513.

Kaur, J., and Debnath, J. (2015). Autophagy at the crossroads of catabolism and anabolism. Nat. Rev. Mol. Cell Biol. *16*, 461–472.

Kawamata, T., Kamada, Y., Suzuki, K., Kuboshima, N., Akimatsu, H., Ota, S., Ohsumi, M., and Ohsumi, Y. (2005). Characterization of a novel autophagy-specific gene, ATG29. Biochem. Biophys. Res. Commun. *338*, 1884–1889.

Kawamata, T., Kamada, Y., Kabeya, Y., Sekito, T., and Ohsumi, Y. (2008). Organization of the Pre-autophagosomal Structure Responsible for Autophagosome Formation. Mol. Biol. Cell *19*, 2039–2050.

Keppler, A., Gendreizig, S., Gronemeyer, T., Pick, H., Vogel, H., and Johnsson, K. (2003). A general method for the covalent labeling of fusion proteins with small molecules in vivo. Nat. Biotechnol. *21*, 86–89.

Kijanska, M., Dohnal, I., Reiter, W., Kaspar, S., Stoffel, I., Ammerer, G., Kraft, C., and Peter, M. (2010). Activation of Atg1 kinase in autophagy by regulated phosphorylation. Autophagy *6*, 1168–1178.

Kinz-Thompson, C.D., Bailey, N.A., and Gonzalez, R.L. (2016). Precisely and Accurately Inferring Single-Molecule Rate Constants. Methods Enzymol. *581*, 187–225.

Klionsky, D.J. (2007). Autophagy: from phenomenon to mechanism in less than a decade. Nature *8*.

Klionsky, D.J., Cregg, J.M., Dunn, W.A., Emr, S.D., Sakai, Y., Sandoval, I. V., Sibirny, A., Subramani, S., Thumm, M., Veenhuis, M., et al. (2003). A unified nomenclature for yeast autophagy-related genes. Dev. Cell *5*, 539–545.

Köfinger, J., Ragusa, M.J., Lee, I.H., Hummer, G., and Hurley, J.H. (2015). Solution structure of the Atg1 complex: Implications for the architecture of the phagophore assembly site. Structure *23*, 809–818.

Kraft, C., Kijanska, M., Kalie, E., Siergiejuk, E., Lee, S.S., Semplicio, G., Stoffel, I., Brezovich, A., Verma, M., Hansmann, I., et al. (2012). Binding of the Atg1/ULK1 kinase to the ubiquitin-like protein Atg8 regulates autophagy. EMBO J. *31*, 3691–3703.

Kudalkar, E.M., Davis, T.N., and Asbury, C.L. (2016a). Total Internal Reflection Fluorescence Microscopy. Cold Spring Harb. Protoc. *2016*, 62–69.

Kudalkar, E.M., Deng, Y., Davis, T.N., and Asbury, C.L. (2016b). Coverslip cleaning and functionalization for total internal reflection fluorescence microscopy. Cold Spring Harb. Protoc. *2016*, 459–465.

Li, P., Banjade, S., Cheng, H.C., Kim, S., Chen, B., Guo, L., Llaguno, M., Hollingsworth, J. V., King, D.S., Banani, S.F., et al. (2012). Phase transitions in the assembly of multivalent signalling

proteins. Nature *483*, 336–340.

Lynch-Day, M.A., and Klionsky, D.J. (2010). The Cvt pathway as a model for selective autophagy. FEBS Lett. *584*, 1359–1366.

Mao, K., Chew, L.H., Inoue-Aono, Y., Cheong, H., Nair, U., Popelka, H., Yip, C.K., and Klionsky, D.J. (2013). Atg29 phosphorylation regulates coordination of the Atg17-Atg31-Atg29 complex with the Atg11 scaffold during autophagy initiation. Proc. Natl. Acad. Sci. *110*, E2875–E2884.

Meia, Y., Sua, M., Sonia, G., Salemc, S., Colbert, C.L., and Sinhaa, S.C. (2014). Intrinsically Disordered Regions in Autophagy Proteins. Proteins *82*, 565–578.

Menzies, F.M., Fleming, A., and Rubinsztein, D.C. (2015). Compromised autophagy and neurodegenerative diseases. Nat. Rev. Neurosci. *16*, 345–357.

Mizushima, N. (2010). The role of the Atg1/ULK1 complex in autophagy regulation. Curr. Opin. Cell Biol. *22*, 132–139.

Mizushima, N., and Komatsu, M. (2011). Autophagy: Renovation of cells and tissues. Cell *147*, 728–741.

Mizushima, N., Yoshimori, T., and Ohsumi, Y. (2011). The Role of Atg Proteins in Autophagosome Formation. Annu. Rev. Cell Dev. Biol. *27*, 107–132.

Morishita, H., and Mizushima, N. (2019). Diverse Cellular Roles of Autophagy. Annu. Rev. Cell Dev. Biol. *35*, 1–23.

Nakatogawa, H., Suzuki, K., Kamada, Y., and Ohsumi, Y. (2009). Dynamics and diversity in autophagy mechanisms: Lessons from yeast. Nat. Rev. Mol. Cell Biol. *10*, 458–467.

Noda, N.N., and Inagaki, F. (2015). Mechanisms of Autophagy. Annu. Rev. Biophys. *44*, 101–122.

Noda, T., Tokunaga, C., Ohsumi, Y., Kim, J., Huang, W.-P., Klionsky, D.J., and Baba, M. (2000). Apg9p/Cvt7p is an integral membrane protein required for transport vesicle formation in the Cvt and autophagy pathways. J. Cell Biol. *148*, 465–479.

Onodera, J., and Ohsumi, Y. (2005). Autophagy is required for maintenance of amino acid levels and protein synthesis under nitrogen starvation. J. Biol. Chem. *280*, 31582–31586.

Pan, H., Xia, Y., Qin, M., Cao, Y., and Wang, W. (2015). A simple procedure to improve the surface passivation for single molecule fluorescence studies. Phys. Biol. *12*.

Papinski, D., Schuschnig, M., Reiter, W., Wilhelm, L., Barnes, C.A., Maiolica, A., Hansmann, I., Pfaffenwimmer, T., Kijanska, M., Stoffel, I., et al. (2014). Early Steps in Autophagy Depend on Direct Phosphorylation of Atg9 by the Atg1 Kinase. Mol. Cell *53*, 471–483.

Qi, S., Kim, D.J., Stjepanovic, G., and Hurley, J.H. (2015). Structure of the human Atg13-Atg101 HORMA heterodimer: An interaction hub within the ULK1 complex. Structure *23*, 1848–1857.

Ragusa, M.J., Stanley, R.E., and Hurley, J.H. (2012). Architecture of the atg17 complex as a scaffold for autophagosome biogenesis. Cell *151*, 1501–1512.

Rao, Y., Perna, M.G., Hofmann, B., Beier, V., and Wollert, T. (2016). The Atg1-kinase complex tethers Atg9-vesicles to initiate autophagy. Nat. Commun. *7*.

Reggiori, F., Tucker, K.A., Stromhaug, P.E., and Klionsky, D.J. (2004a). The Atg1-Atg13 complex regulates Atg9 and Atg23 retrieval transport from the pre-autophagosomal structure. Dev. Cell *6*, 79–90.

Reggiori, F., Wang, C.-W., Nair, U., Shintani, T., Abeliovich, H., and Klionsky, D.J. (2004b). Early Stages of the Secretory Pathway, but Not Endosomes, Are Required for Cvt Vesicle and Autophagosome Assembly in Saccharomyces cerevisiae. Mol. Biol. Cell *15*, 2189–2204.

Reggiori, F., Shintani, T., Nair, U., and Klionsky, D.J. (2005). Atg9 Cycles between Mitochondria and the Pre-Autophagosomal Structure in Yeasts. Autophagy *1*, 101–109.

Sekito, T., Kawamata, T., Ichikawa, R., Suzuki, K., and Ohsumi, Y. (2009). Atg17 recruits Atg9 to organize the pre-autophagosomal structure. Genes to Cells *14*, 525–538.

Shintani, T., and Klionsky, D.J. (2004). Cargo proteins facilitate the formation of transport vesicles in the cytoplasm to vacuole targeting pathway. J. Biol. Chem. *279*, 29889–29894.

Stephan, J.S., Yeh, Y.-Y., Ramachandran, V., Deminoff, S.J., and Herman, P.K. (2009). The Tor and PKA signaling pathways independently target the Atg1/Atg13 protein kinase complex to control autophagy. Proc. Natl. Acad. Sci. *106*, 17049–17054.

Stjepanovic, G., Davies, C.W., Stanley, R.E., Ragusa, M.J., Kim, D.J., and Hurley, J.H. (2014). Assembly and dynamics of the autophagy-initiating Atg1 complex. Proc. Natl. Acad. Sci. *111*, 12793–12798.

Suzuki, K., Kirisako, T., Kamada, Y., Mizushima, N., Noda, T., and Ohsumi, Y. (2001). The pre-autophagosomal structure organized by concerted functions of APG genes is essential for autophagosome formation. EMBO J. *20*, 5971–5981.

Suzuki, K., Kubota, Y., Sekito, T., and Ohsumi, Y. (2007). Hierarchy of Atg proteins in pre-autophagosomal structure organization. Genes to Cells *12*, 209–218.

Suzuki, S.W., Yamamoto, H., Oikawa, Y., Kondo-Kakuta, C., Kimura, Y., Hirano, H., and Ohsumi, Y. (2015). Atg13 HORMA domain recruits Atg9 vesicles during autophagosome formation. Proc. Natl. Acad. Sci. *112*, 3350–3355.

Thevelein, J.M., Cauwenberg, L., Colombo, S., De Winde, J.H., Donation, M., Dumortier, F., Kraakman, L., Lemaire, K., Ma, P., Nauwelaers, D., et al. (2000). Nutrient-induced signal transduction through the protein kinase A pathway and its role in the control of metabolism, stress resistance, and growth in yeast. In Enzyme and Microbial Technology, pp. 819–825.

Trakselis, M.A., Alley, S.C., and Ishmael, F.T. (2005). Identification and mapping of protein-protein interactions by a combination of cross-linking, cleavage, and proteomics. Bioconjug. Chem. *16*, 741–750.

Tsukada, M., and Ohsumi, Y. (1993). Isolation and characterization of autophagy-defective mutants of Saccharomyces cerevisiae. FEBS *333*, 169–174.

Yamamoto, H., Kakuta, S., Watanabe, T.M., Kitamura, A., Sekito, T., Kondo-Kakuta, C., Ichikawa, R., Kinjo, M., and Ohsumi, Y. (2012). Atg9 vesicles are an important membrane source during early steps of autophagosome formation. J. Cell Biol. *198*, 219–233.

Yamamoto, H., Fujioka, Y., Suzuki, S.W., Noshiro, D., Suzuki, H., Kondo-Kakuta, C., Kimura, Y., Hirano, H., Ando, T., Noda, N.N., et al. (2016). The Intrinsically Disordered Protein Atg13 Mediates Supramolecular Assembly of Autophagy Initiation Complexes. Dev. Cell *38*, 86–99.

Yeh, Y.Y., Wrasman, K., and Herman, P.K. (2010). Autophosphorylation within the Atg1 activation loop is required for both kinase activity and the induction of autophagy in Saccharomyces cerevisiae. Genetics *185*, 871–882.

Yeh, Y.Y., Shah, K.H., and Herman, P.K. (2011). An Atg13 protein-mediated self-association of the Atg1 protein kinase is important for the induction of autophagy. J. Biol. Chem. *286*, 28931–28939.

Yuan, W., Guo, S., Gao, J., Zhong, M., Yan, G., Wu, W., Chao, Y., and Jiang, Y. (2017). General control nonderepressible 2 (GCN2) kinase inhibits target of rapamycin complex 1 in response to amino acid starvation in saccharomyces cerevisiae. J. Biol. Chem. *292*, 2660–2669.